# Glaciations on ophiolite terrain in the North Pindus mountains, Greece: new geomorphological insights and preliminary $^{36}$Cl exposure dating

Aris D. Leontaritis[1*], Kosmas Pavlopoulos[2], Shasta M. Marrero[3], Adriano Ribolini[4], Philip D. Hughes[5], Matteo Spagnolo[6],

*1. Department of Geography, Harokopio University of Athens, 17671, Athens Greece*

*2. Department of Geography and Planning, Sorbonne University Abu Dhabi, 38044 , A.D. UAE*

*3. School of Earth and Environmental Sciences, Cardiff University, Main Building, Cardiff, CF10 3AT, UK*

*4. Department of Earth Sciences, University of Pisa, 56126, Pisa, Italy*

*5. Department of Geography, School of Environment, Education and Development, The University of Manchester, Manchester, M13 9PL, England, UK*

*6. School of Geosciences, University of Aberdeen, AB24 3UF, Aberdeen, UK*

*Correspondence (aris.leontaritis@gmail.com)

## Abstract

*A glacial geomorphological analysis of three valleys on Mt Mavrovouni (North Pindus Mountains, Greece) is presented alongside a pilot study using cosmogenic $^{36}$Cl to obtain surface exposure ages from iron-rich ophiolite glacial and periglacial boulders. At least three distinct morphostratigraphic units of glacial (moraines) and periglacial (relict pronival ramparts) origin have been identified. Four $^{36}$Cl surface exposure ages were obtained from the stratigraphically youngest glacial and periglacial deposits. Although this limited dataset with relatively large uncertainties cannot support a robust geochronology, the ages are consistent with the $^{36}$Cl-based chronologies of limestone-derived moraines on Mt Tymphi (NW Greece) and Mt Chelmos (S Greece), confirming that the last glaciers on this massif formed during the Last Glacial Maximum as also indicated by other studies in the Pindus mountains. At the same time it provides confidence in the suitability of $^{36}$Cl dating for iron-rich samples, such as ophiolites, using an updated $^{36}$Cl model that incorporates improved production rates for iron spallation. The presented preliminary chronology of moraines and*

*pronival ramparts is based on those ages as well as on local and regional morphostratigraphic correlations. The stabilisation of the most extensive Late Pleistocene glaciers took place during the Last Glacial Maximum, at 27.0 ± 6.5 ka whereas the presence of pronival ramparts dated at 20.2 ± 4.8 ka suggests persisting cold and arid conditions. Older, still undated glacial deposits exist lower in the valleys which can be attributed to the Middle Pleistocene major glaciation phases (MIS 12 / MIS 6), based on their relative morphostratigraphic position within the glacial sedimentary sequence.*

**Key words**: glacial geomorphology; Greece; ophiolites; cosmogenic $^{36}$Cl exposure age dating, Last Glacial Maximum

# 1 Introduction

The former extents of mid-latitude mountain glaciers represent a sensitive record of past changes in climate as their relatively small size means that they rapidly change volume in response to mass balance changes caused by regional or local climatic changes (Bahr et al., 1998; Oerlemans, 2005; Woodward, 2009; Vogiatzakis, 2012). Mapping and dating of past ice margins, documented by glacial sediments and landforms, not only provides insights into past climate change but also provides valuable information for understanding landscape evolution (Owen et al., 2002; Svendsen et al., 2004).

In order to compare palaeoglaciers in different geographical settings, a useful tool is the Equilibrium Line Altitude (ELA), i.e. the elevation of a glacier where annual accumulation and ablation are equal, which is governed by air temperature and precipitation (Ohmura and Boettcher, 2018). Moreover, as temperatures at a regional level may practically depend on elevation rather than latitude (e.g. Greece, central Italy; Katsoulakos and Kaliampakos, 2014; Papada and Kaliampakos, 2016), ELAs in this case can be considered to be mainly governed by precipitation and therefore constitute a direct precipitation proxy.

Evidence of former glaciation is abundant throughout the mountains of Greece (e.g. Niculescu, 1915; Mistardis, 1935; Hughes et al., 2006a, 2006b; Styllas, 2018; Leontaritis et al., 2020 and references therein). The Pindus Mountains in north-western Greece is historically a key-region for the study of the glacial history of the Balkans and the Mediterranean (Woodward and Hughes, 2011). The first pioneer geographical studies reporting glacial features took place early in the 20th century (Niculescu, 1915; Bourcart, 1922; Louis, 1926; Sestini, 1933; Mistardis, 1935) whereas systematic geomorphological mapping was initiated decades later (Palmentola et al., 1990; Boenzi et al., 1992). Hughes et al. (2006a) used U-series dating on the most extensive moraines on Mt Tymphi to show that the most intense glacial phases correspond to MIS 6 (Vlasian Stage: ca. 190-130 ka) and further back to MIS 12 (Skamnellian Stage: ca. 480-430 ka) during the Middle Pleistocene. The stratigraphically younger Late Pleistocene moraines on Mt Tymphi were only recently dated to the Last Glacial Maximum (LGM: 27.5-23.3 ka; Hughes and Gibbard, 2015) with $^{36}$Cl surface exposure dating on limestones (Allard et al., 2020). Surface exposure ages from Mt Chelmos in southern Greece ($^{36}$Cl ages from limestones ; Figure 1) indicate that this glacial phase is likely to correspond to an interval c. 5-10 ka prior to the global LGM (Pope et al., 2017). Today, the Late-glacial (17.5-11.7 ka) features of the region remain largely neglected because their presence is limited to the ophiolitic Mt Smolikas (Leontaritis et al., 2020; Figure 1), with its peculiar lithology preventing the dating of its moraines with absolute dating methods (Woodward and Hughes, 2011). Thus, the response of glaciers in the Pindus Mountains to the cold events of this interval remains poorly elucidated. A lingering question is if this evidence supports a local (intra-Pindus) and regional (across Greece) chronological and morphostratigraphic framework to describe Quaternary glaciations or if local topographic and climatic factors dominated glacial growth during specific glacial phases like for example Holocene glaciations in Montenegro (Hughes, 2007; 2010a).

Terrestrial cosmogenic nuclides have been used to date glacial landforms all over the world (e.g. Gosse et al., 1995; Finkel et al., 2003; Balco and Schafer, 2006; D'Arcy et al., 2019; Anjar et al., 2021), but the ophiolitic lithology in the Pindus restricts possible nuclides to only $^{3}$He and $^{36}$Cl (Leontaritis, 2021), so $^{36}$Cl was chosen due to the ability to handle any possible variability in the lithology (e.g. lack of sufficient olivines; see Ivy-Ochs and Kober, 2008). Although $^{36}$Cl exposure dating has been successfully applied on serpentinized harzburgites to date glacial deposits (see Sarikaya et al., 2008), it has not yet been fully characterised. This is the only option for carbonate rocks as well and so has been used to date the above-mentioned moraines in the limestone massifs of Mt Tymphi (Allard et al., 2020) and Mt Chelmos (Pope et al., 2007). However, carbonate rocks are also more susceptible than others to the effects of surface erosion, so this potentially increases the uncertainty associated with those ages (Allard et al., 2020, Sarikaya et al., 2020).

The aim of this paper is to establish a preliminary chronology of the glacial deposits on Mt Mavrovouni in the Pindus Mountains based on a detailed glacial geomorphological study and the preliminary timing constraint of its ophiolite-dominated glacial deposits through a pilot study using cosmogenic $^{36}$Cl surface exposure dating. The main objective is to confirm that the formation of the stratigraphically youngest glacial deposits in this massif falls within the LGM as suggested by morphostratigraphic correlations of moraines within the Pindus mountains (Mt Tymphi, Mt Smolikas and Mt Mavrovouni; Leontaritis, 2021; Figure 1). Thus, in this pilot study, sampling was limited to these sediments, initially correlated with Late Pleistocene glacial activity. The small number of ages allows only for a preliminary timing constraint of the respective cold events on Mt Mavrovouni and additional data will still be needed to establish a tighter and more reliable chronology. However, the presented chronology is sufficient to confirm the viability of cosmogenic $^{36}$Cl surface exposure dating using new production rates for Fe spallation on iron-rich ophiolites. Given the fact that some

of the highest peaks of the Pindus and the wider Balkans are formed in this lithology, it sets the agenda for future research on similar glaciated terrains.

## 2 Regional Setting

Mt Mavrovouni is located in the north Pindus Mountains in NW Greece (Figure 1), only 20km to the east/southeast of Mt Tymphi (2497m a.s.l.) and 30km to the southeast of Mt Smolikas (2637m a.s.l.). Its highest peak (Flega) reaches an altitude of 2157m a.s.l.; considerably lower than the neighbouring mountains. Mt Mavrovouni, alongside, Mt Smolikas and Mt Vasilitsa (2248 m a.s.l.) belongs to the Northern Pindus ophiolitic complex, part of a nappe which is tectonically overthrust onto the Eocene flysch of the Pindus Zone (Dupuy et al. 1984). In particular, Mt Mavrovouni belongs to the Dramala Complex subunit which represents oceanic mantle and part of its crustal sequence (Pelletier et al., 2008). It primarily consists of slightly to highly serpentinized harzburgites of Mid-Jurassic age while subordinate lithologies include dunite, pyroxenite and a range of ultramafic cumulate rocks (Jones and Robertson, 1991; Robertson, 2002; Pelletier et al., 2008). Mesozoic limestones and Palaeozoic crystalline schists are also present locally, at the overthrust nappe of the ophiolitic complex (IGME, 1959).

In common with its ophiolitic neighbours, Mt Mavrovouni presents a less complex physiography compared with the limestone dominated Mt Tymphi, as it is a generally rounded mountain with many steep V-shaped valleys and only a few and relatively short cliffs. Evidence of glaciation is present on its northern slopes. The glacial sedimentary morphosequence (i.e. the spatial distribution of moraines along a valley indicating phases of glacial advance/standstill) is fragmented with the exception of the U-shaped Mnimata valley (Figure 2). Focus was given on constraining the timing of processes that formed the highest and therefore stratigraphically youngest glacial/periglacial deposits in the Mnimata valley,

which, according to evidence elsewhere in Greece, are expected to be Late Pleistocene in age (Leontaritis et al., 2020 and references therein).

No glaciers, permafrost or permanent snow fields are present today. Snow cover on the northern slopes above 1800m a.s.l. lasts from early December to late May. Direct climatological data are available from four high-altitude local stations at distances <20km (Vovousa - 1000m a.s.l., Greveniti - 976m a.s.l., Elatochori - 1014m a.s.l. and Metsovo - 1160m a.s.l.; precipitation data from Fotiadi et al., 1999; temperature data from Gouvas and Sakellariou, 2011; reference period >20yr).. Extrapolating temperature data to a representative altitude of 2000m a.s.l. with a lapse rate of 0.6°C per 100m of altitude (Leontaritis, 2021) estimated the mean annual and monthly (July, January) temperatures at 4.5$^{o}$C, 13.8$^{o}$C and -3.0$^{o}$C respectively. Precipitation data were extrapolated using a precipitation gradient of 55 mm per 100 m altitude for this area (Hughes, 2004) and the mean annual precipitation at 2000m a.s.l. is expected to exceed 2000mm (Leontaritis, 2021) confirming earlier suggestions by Furlan (1977).

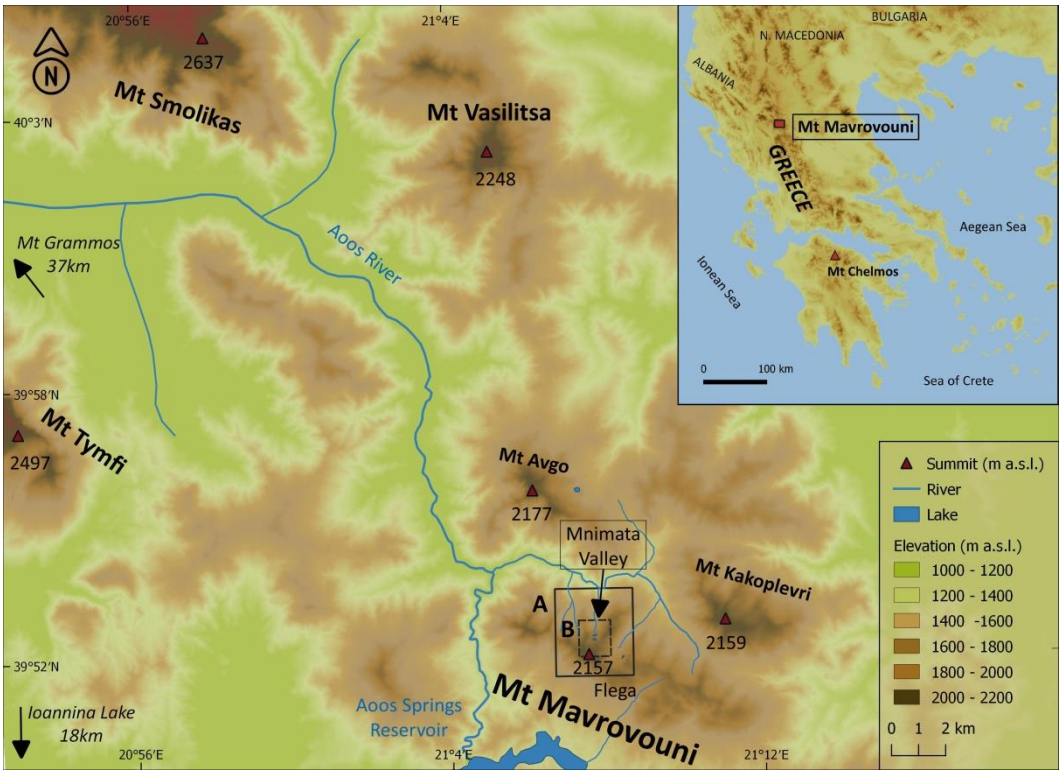

*Figure 1. Map of the study area on Mt Mavrovouni and location of the massif in the southern tip of the Balkan Peninsula (up-right inset map). Detailed glacial geomorphological maps of the areas denoted by boxes A and B are given in Figure 4 and Figure 6, respectively.*

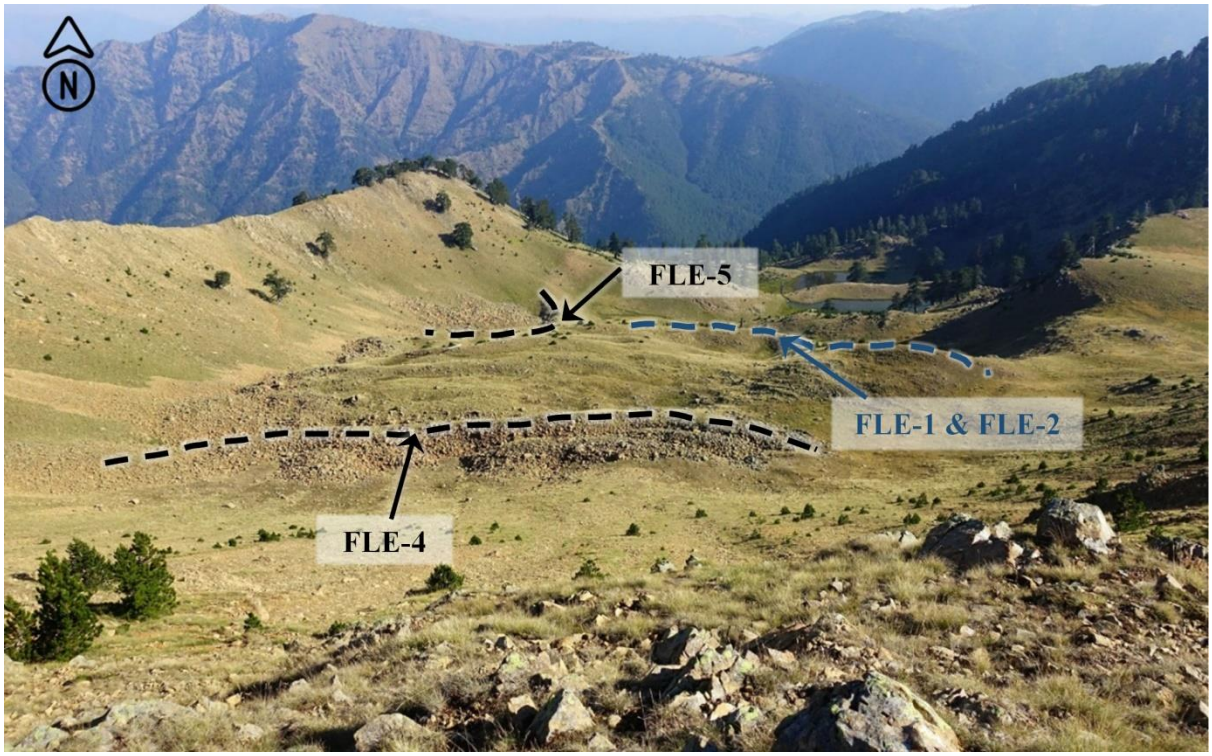


*Figure 2. The Mnimata U-Shaped valley and the glacial/periglacial sedimentary sequence. Sample locations on terminal moraine (dashed blue line) and pronival rampart ridges (dashed black lines) are denoted. Photo looking north from the Flega Peak at 2157 m a.s.l. (Photo: August 2016).*

# 3 Methods

## 3.1 Geomorphological mapping

Geomorphological mapping was conducted following the principles of the idealised approach proposed by Chandler et al. (2018) for glacial geomorphological mapping in alpine environment which involves remotely-sensed data and field mapping. Accordingly, reconnaissance analysis was performed on available topographic maps (e.g. Anavasi, 2016; Open Street Maps), the regional 1:50,000 Geological Sheets of the Greek Institute for Geological and Mineral Exploration (IGME, 1959), and high-resolution satellite imagery

(Google Earth, Bing Maps). The Digital Elevation Model was provided by the National Cadastre at a spatial resolution of 5m. In the field, the reconnaissance sketch-map was refined and glacial, glaciofluvial and periglacial landforms and sediment deposits were mapped and recorded using a commercial GPS/Glonass device (Garmin 64s) over three fieldtrips in the summers of 2016, 2017 and 2018. Additionally, UAV-captured (Unoccupied Aerial Vehicle) aerial photos and videos were taken from the upper Mnimata valley. The digital mapping and the creation of the glacial geomorphological maps were conducted in the open source QGIS environment.

### 3.2 Morphostratigraphic classification of glacial and periglacial features

In this paper, we used morphostratigraphic classification of the different glacial and periglacial features following the principles in Hughes (2010b). Relict pronival ramparts (periglacial or transitional units) were distinguished from moraines using multiple identification criteria (see Hedding and Sumner, 2013; Matthews et al., 2017 and references therein). Units were separated by morphostratigraphic criteria such as relative stratigraphic position, elevation, sediments composition (e.g. clasts size and shape, presence of fines), evidence of exhumation and soil development. Local (i.e. within the same massif) and regional (e.g. within NW Greece) morphostratigraphic correlations allowed the utilization of spatial relationships between individual glacial/periglacial landforms in order to extrapolate existing chronologies of the Pleistocene glacial sequence. Due to the limited availability of dateable sites or material this approach has been successfully applied in glacial geomorphology worldwide, underlying many glacier reconstructions (e.g. Lowe and Walker, 1997; Chadwick et al., 1997; Richards et al., 2000; Benn and Ballantyne, 2005; Lukas, 2006).

### 3.3 Cosmogenic $^{36}$Cl surface exposure dating

The ophiolitic lithology of the Northern Pindus Mountains (Mt Mavrovouni, Mt Smolikas, Mt Vasilitsa and Mt Grammos; Figure 1) has so far prevented the age control of

glacial deposits with absolute dating methods (Hughes et al., 2006a; Woodward and Hughes, 2011). In particular, widely used techniques for dating glacial deposits such as cosmogenic $^{10}$Be or $^{26}$Al surface exposure dating, luminescence and U-series are unsuitable for such lithologies due to the complete lack of quartz, feldspar or secondary calcites (Fuchs and Owen, 2008; Ivy-Ochs and Kober, 2008). In theory, cosmogenic $^{36}$Cl surface exposure dating can be used for any rock type under most conditions (Ivy-Ochs and Kober, 2008) and it has successfully been applied to date glacial deposits on ophiolites and specifically on serpentinized harzburgites on Mt Sandiras, SW Turkey (Sarikaya et al., 2008). In such lithologies, the relatively high concentrations of iron (Fe) and native Cl means that the main production of cosmogenic $^{36}$Cl is expected from neutron capture by $^{35}$Cl and spallation reactions in Fe (Gosse and Phillips, 2001; Marrero et al., 2016a). Because spallation from Fe usually comprises <2% of total production in most rocks (Marrero et al., 2016a), production from this pathway was not explicitly calibrated in earlier large-scale $^{36}$Cl calibration efforts (Phillips et al., 2001; Swanson and Caffee, 2001; Schimmelpfennig et al., 2011; Marrero et al., 2016a), leading to a potential for larger uncertainties in high-Fe samples (Gosse and Phillips, 2001; Asimov and Ivy-Ochs, 2009; Marrero et al., 2016a; Moore and Granger, 2019). This study incorporates new Fe-spallation production rates from Moore and Granger (2019) in order to reduce uncertainty on high-Fe sample ages (Anjar et al., 2021).

### 3.3.1 Sample collection and characterization

The sampling strategy for $^{36}$Cl cosmogenic nuclide dating was influenced by the objective of this study which was to confirm that the last glaciation on Mt Mavrovouni formed during the last glacial cycle as well as by the limited resources available for $^{36}$Cl analyses. Therefore, this study focused from a geochronological point of view on the stratigraphically youngest glacial/periglacial deposits on Mt Mavrovouni according to the geomorphological analysis. More specifically, sampling was aimed at the sequence of glacial/periglacial deposits in the

upper Mnimata valley (Figure 2). Four samples were collected following the principles in Gosse and Phillips (2001). Two samples (FLE-1 and FLE -2) were collected from the ridge of a terminal moraine at the lowermost part of this sequence whereas two more samples were collected from the ridges of two relict ramparts immediately below the cirque walls (FLE-4 and FLE-5). The approach to date the stratigraphically youngest and oldest deposits in this sequence was followed in an effort to best exploit the small number of available analyses in order to constrain the timing of this cold stage.

All sampled boulders are of ophiolitic lithology. Samples were obtained with the use of a hammer and chisel from the upper 2-3cm of a flat rock surface as far away as possible from the boulder's edges to minimise edge effects (Gosse and Phillips, 2001; Masarik and Wieler, 2003; Darvill, 2013). Topographic shielding for the four samples was determined with the use of an open-access DEM-based GIS toolbox dedicated to the calculation of cosmic radiation topographic shielding for discrete sample points on the available 5m-resolution DEM (Li, 2018; available online at https://web.utk.edu/~yli32/programs.html).

The highly-serpentinized ophiolitic rocks show very limited signs of weathering implying very low surface erosion rates as also indicated by ice-polished bedrock with well-preserved striations below the lower Flega tarn (Figure 3). A surface erosion correction factor for the calculation of the final ages was thus not considered. Also, information about contemporary and Late Pleistocene snow cover is not available so this was not considered. Styllas et al. (2018) showed that on Mt Olympus even when quite a significant snow correction factor was considered (0.94), the resulting deviations on calculated Late-glacial exposure ages were in the scale of a few hundred years. Taking into consideration the calculated age uncertainties, such deviations are practically negligible and the calculated (non-corrected and thus minimum) ages can be associated to the age of moraine deposition. The location and characteristics of the collected samples are summarised in Table 1.

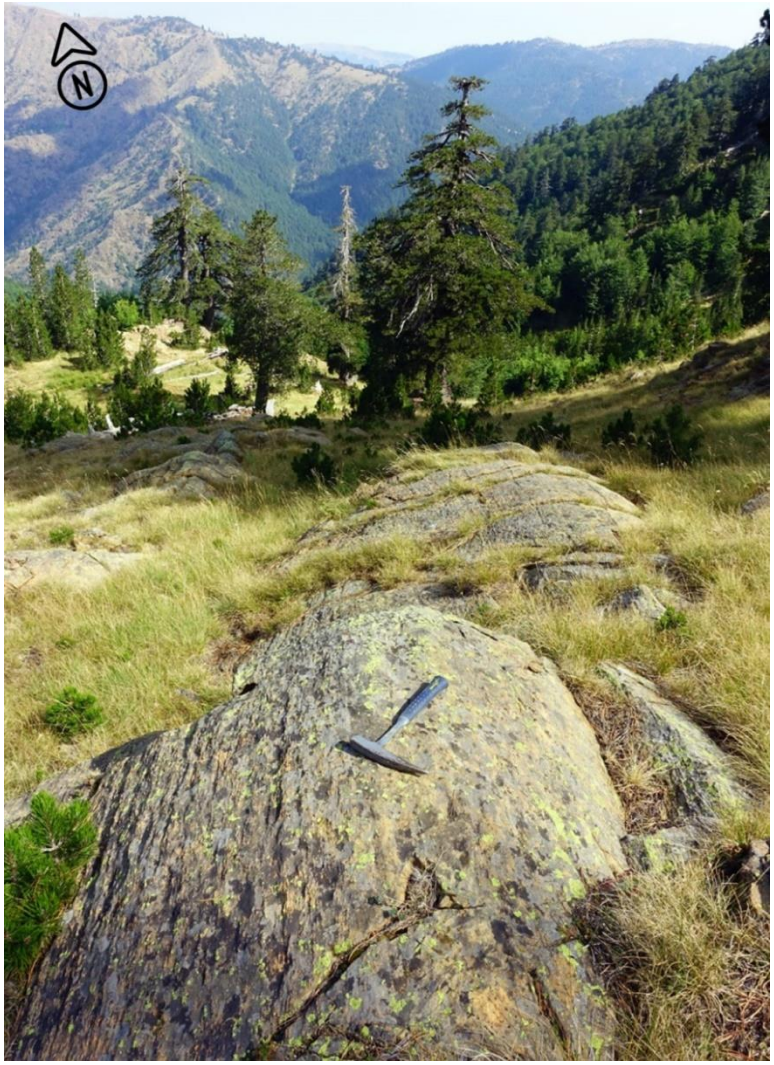

*Figure 3. Ice-polished bedrock with well-preserved striations below the lower Flega tarn is indicative of very low surface erosion rates. This outcrop of ice-polished bedrock was exposed after the glacier's retreat and as indicated by field evidence the preservation of the striations should not be attributed to soil cover protection: soil in this upper part of the massif has been developed mostly on depressions whereas rocky exertions generally lack any soil cover (Photo August 2016).*

*Table 1. Location and characteristics of collected $^{36}Cl$ samples.*

| Sample ID | Latitude (N°) | Longitude (E°) | Elevation (m a.s.l.) | Sample thickness (cm) | Sample Density (g cm$^{-3}$) | Topographic Shielding Factor (-) |
|---|---|---|---|---|---|---|
| FLE-1 | 39.8737 | 21.1204 | 2017 | 2.0 | 2.7 | 0.978 |
| FLE-2 | 39.8735 | 21.1205 | 2017 | 2.5 | 2.7 | 0.985 |
| FLE-4 | 39.8725 | 21.1190 | 2038 | 3.0 | 2.7 | 0.978 |

| | | | | | | |
|---|---|---|---|---|---|---|
| FLE-5 | 39.8749 | 21.1193 | 1978 | 3.0 | 2.7 | 0.989 |

### 3.3.2 Samples preparation AMS measurements

Rock samples were crushed and sieved at the National Technical University of Athens. Subsequently, the 250-500 μm fraction underwent chemical processing and measurement at the Purdue Rare Isotope Measurement Laboratory (PRIMElab) at Purdue University. Samples were leached in 5% dilute nitric acid ($HNO_3$) several times, had ~1 mg of chlorine carrier added (Table 2), dissolved with concentrated hydrofluoric (HF) and nitric acids, heated in a 60ºC water bath, then fluoride by-products were removed by centrifugation. Silver chloride (AgCl) was precipitated from samples, then it was purified using barium nitrate [$Ba(NO_3)_2$] and anion columns before being dried and pressed into cathodes.

*Table 2. AMS analytical data for $^{36}Cl$ samples. Standard Deviation given in parentheses. *Carrier: $^{35}Cl/^{37}Cl$ ratio 273. Total Cl content was determined using standard isotope dilution calculations (Desilets et al., 2006).*

| Sample ID | Mass (g) | Carrier* added (mg Cl) | $^{36}Cl/Cl$ ratio ($x10^{-15}$) | $^{35}Cl/^{37}Cl$ stable ratio | Cl content (ppm) | Measured $^{36}Cl$ (atoms • $g^{-1}$) |
|---|---|---|---|---|---|---|
| FLE-1 | 30.242 | 1.0805 | 108.5 (4.2) | 5.48 (0.03) | 58.89 (0.76) | 177,500 (7,100) |
| FLE-2 | 30.188 | 1.0864 | 186.7 (5.8) | 5.51 (0.06) | 58.57 (1.62) | 307,700 (10,900) |
| FLE-4 | 30.213 | 1.0841 | 161.7 (5.1) | 3.90 (0.03) | 188.59 (6.67) | 622,800 (27,000) |
| FLE-5 | 30.221 | 1.0676 | 368.0 (8.4) | 8.50 (0.02) | 23.43 (0.22) | 386,200 (8,900) |

The $^{36}Cl$ to total stable chlorine ratio ($^{36}Cl/Cl$) and the stable $^{35}Cl/^{37}Cl$ ratio were measured by Accelerator Mass Spectrometry (AMS) on the 8 MV tandem accelerator at PRIME Lab, normalising $^{36}Cl/Cl$ measurements to NIST reference material SRM 4943 standards (Sharma et al., 1990). The AMS data for the samples alongside the calculated total Cl content and $^{36}Cl$ concentration for each sample are summarised in Table 2.

### 3.3.3 Cosmogenic $^{36}Cl$ exposure age calculations

The exposure ages of the samples were calculated using the CRONUScalc $^{36}$Cl Exposure Age Calculator v2.2 (original code available in Bitbucket repository: v2.2, https://bitbucket.org/cronusearth/cronus-calc/; Marrero et al., 2016b). The time-dependent and nuclide-dependent Lifton-Sato-Dunai scaling (LSDn) scaling framework (Lifton et al., 2014) was selected, due to its fit to calibration data (Phillips et al., 2016). This model is based on equations from a nuclear physics model and incorporates dipole and non-dipole magnetic field fluctuations and solar modulation and includes nuclide-specific scaling factors (Lifton et al., 2014; Marrero et al., 2016b). Production rates used in the calculator are from Marrero et al. (2016a; 2021), with newly incorporated $^{36}$Clproduction rates from iron spallation from Moore and Granger (2019), as described in Anjar et al. (2021).

# 4 Results

## 4.1 Glacial and periglacial evidence

Detailed mapping was conducted in three north-oriented glacial valleys on Mt Mavrovouni (Figure 4). All valleys extend between the main NW-SE watershed at c. 2100m a.s.l. and c. 1300-1200m a.s.l where they converge to a main valley. No trace of glaciation was identified on the southern slopes. The glacial and periglacial features identified in the three valleys were morphostratigraphically classified upon elevation, relative stratigraphic position, and degree of degradation (e.g. moraine dismantling) into three distinct units which are summarised in Table 3. Unit 1 consists of the stratigraphically older glacial features at relatively low elevations within the valleys characterised by exhumed and relatively eroded moraines. Unit 2 represents a group of well-preserved moraines with distinct depositional limits which are limited to higher elevations within the cirques. On the contrary, Unit 3 deposits have been classified as a group of periglacial features (relict rampart ridges) due to their proximity to the cirque walls, shape and composition (domination of large angular boulders and lack of fines).

281 *Table 3. Morphostratigraphic classification of glacial and periglacial features on Mt Mavrovouni*

| Valley | Unit 1 | Unit 2 | Unit 3 |
|---|---|---|---|
| Flega | Lateral Moraine<br>1740 - 1840m a.s.l. | Scattered glacial boulders<br>Moraine damming a lake<br>1880-1920m a.s.l. | - |
| Mnimata | Ice-polished bedrock / Glacial boulders/ Tarns<br>1900 – 1950m a.s.l. | Terminal and hummocky moraines<br>2000 – 2040m a.s.l. | Pronival Ramparts<br>1980 - 2050m a.s.l. |
| Arkoudolakos (Bear) | Lateral Moraines<br>1500 – 1660m a.s.l.<br>1470 – 1510m a.s.l. | Scattered erratic boulders and till with indistinct depositional limits<br>1800 – 1900m a.s.l. | - |

282

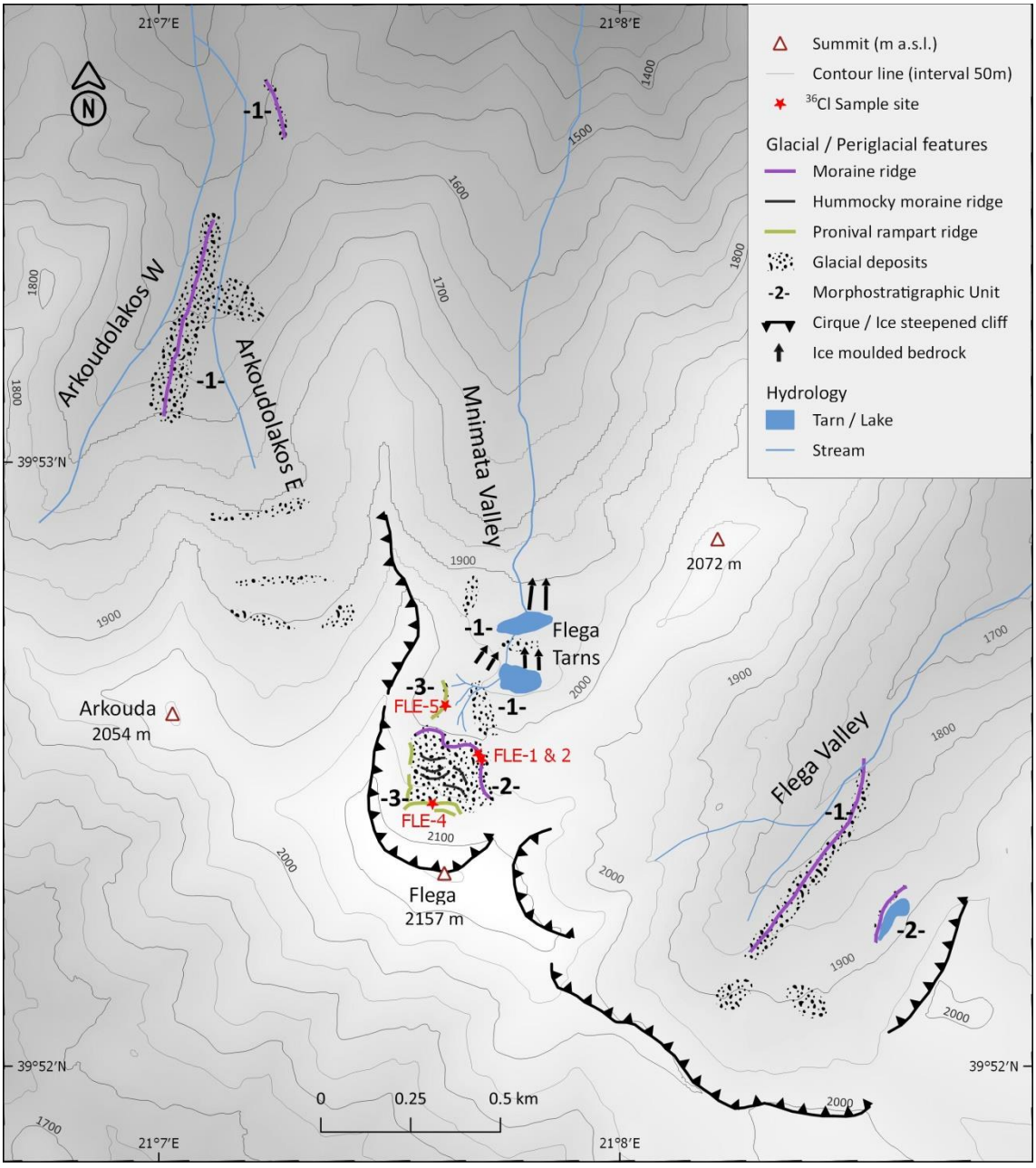


283

*Figure 4. Glacial geomorphological map of the study area on Mt Mavrovouni (Panel A in Figure 1).*

### 4.1.1 Mnimata (Flega Tarns) Valley

The Mnimata glacial valley extends below the summit of Mt Mavrovouni (Flega Peak at 2157m a.s.l.) with a north orientation (Figure 4). It is typically U-shaped and headed by an ice-steepened, and well-developed cirque (Figure 5a). A detailed glacial geomorphological map of the valley is shown in Figure 6 whereas an aerial video captured with an UAV can be seen here. The upper valley is characterised by a clearly shaped and well-preserved glacial/periglacial sequence of deposits between 2050 and 2000m a.s.l., which is a focal point of this research (Figure 5). The lower limit of the sequence is defined by a well-shaped terminal moraine (Unit 2 in Table 3). Two samples for $^{36}$Cl surface exposure dating were taken from the moraine crest at 2017m a.sl. (FLE-1 and FLE-2 in Figure 5a, Figure 6). The middle part of the sequence is characterised by hummocky moraine with scattered subrounded glacial boulders that formed upon glacial retreat. These deposits have likely undergone further permafrost-related creep, though without any typical rock glacier features as ridges or lobes.

Higher in the valley, there is a sharp and continuous boulder ridge with minimum soil development and mainly composed of large angular boulders that have been deposited at the centre of the cirque-floor. These boulders are considerably different in shape compared to the glacially worked and therefore subrounded boulders found lower in the main sedimentary unit (Unit 2 in Table 3) whereas soil development is minimal compared to the Unit 2 moraines. For these reasons, these deposits are ascribed to a distinct younger stratigraphic unit (Unit 3 in Table 3, Figure 4 and Figure 6). A sample was taken from a well-stabilised boulder on the crest of these deposits at 2038m a.s.l. (FLE-4 in Figure 5b, Figure 6). Two minor crests of similar deposits are nested in the eastern part of the main ridge (Figure 5b). The main ridge along with the two minor crests of the angular deposits are interpreted as

pronival ramparts that formed after the formation of the main sedimentary unit (Unit 2 in Table 3,) during persisting cold conditions that were too arid for the development of a glacier but sufficiently humid for the formation of a permanent snow (nevé) field. Local topography and shading from the cirque-walls must have favoured the formation of this nevé field. Further up-valley, no boulders or clasts can be found on the grassy scree-covered slope, supporting the hypothesis of the formation of a pronival rampart during prevailing cold conditions with increased debris supply due to freeze-thaw weathering of the cirque walls.

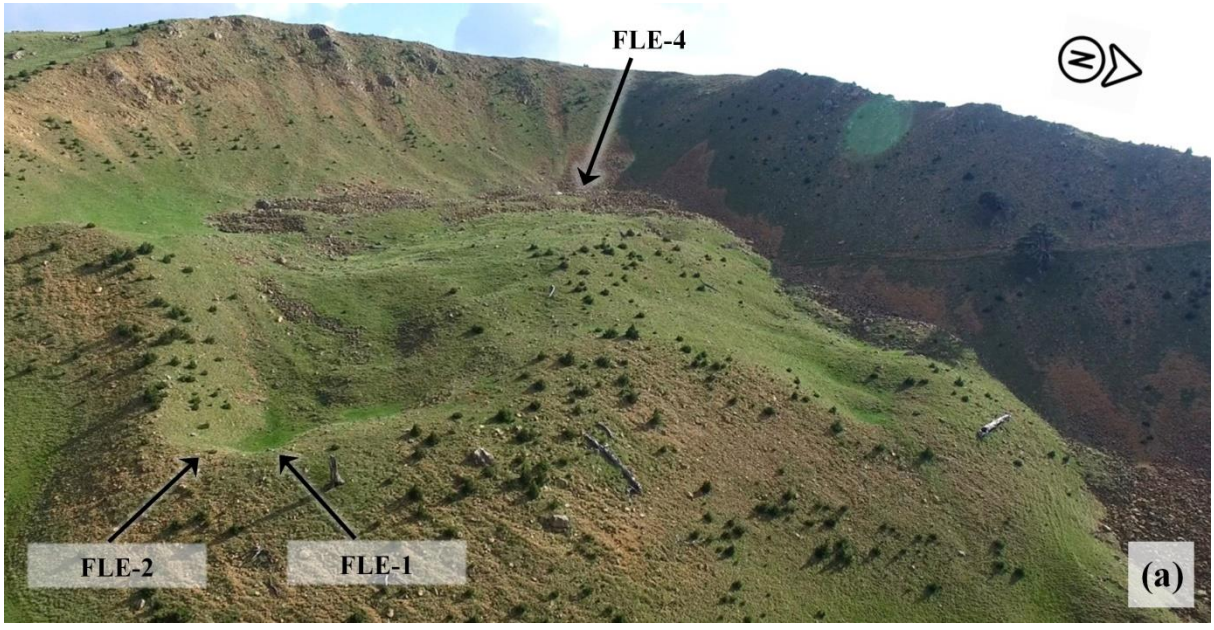


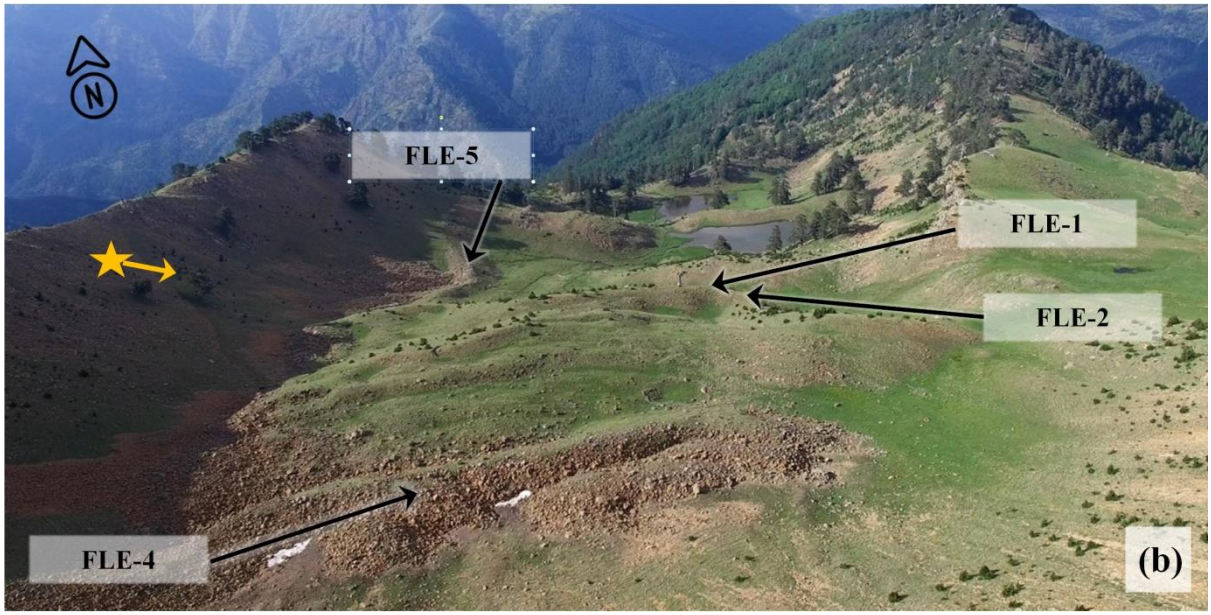

*Figure 5. The upper Mnimata valley and the glacial/periglacial sequence along with sample locations for $^{36}Cl$ dating: a) (Top): Looking up valley. Notice the Unit 2 terminal moraine delimiting this set of deposits in the foreground and the well-developed cirque; b) (Bottom): Looking down valley. Unit 3 pronival deposits can be seen in the foreground along with the denoted sample location. In the background there are the Flega tarns sitting in ice-scoured hollows on the impermeable bedrock. Yellow star and arrow denote shooting location and orientation of Figure 7b. (Aerial Photos: George Panayiotopoulos, June 2019)*

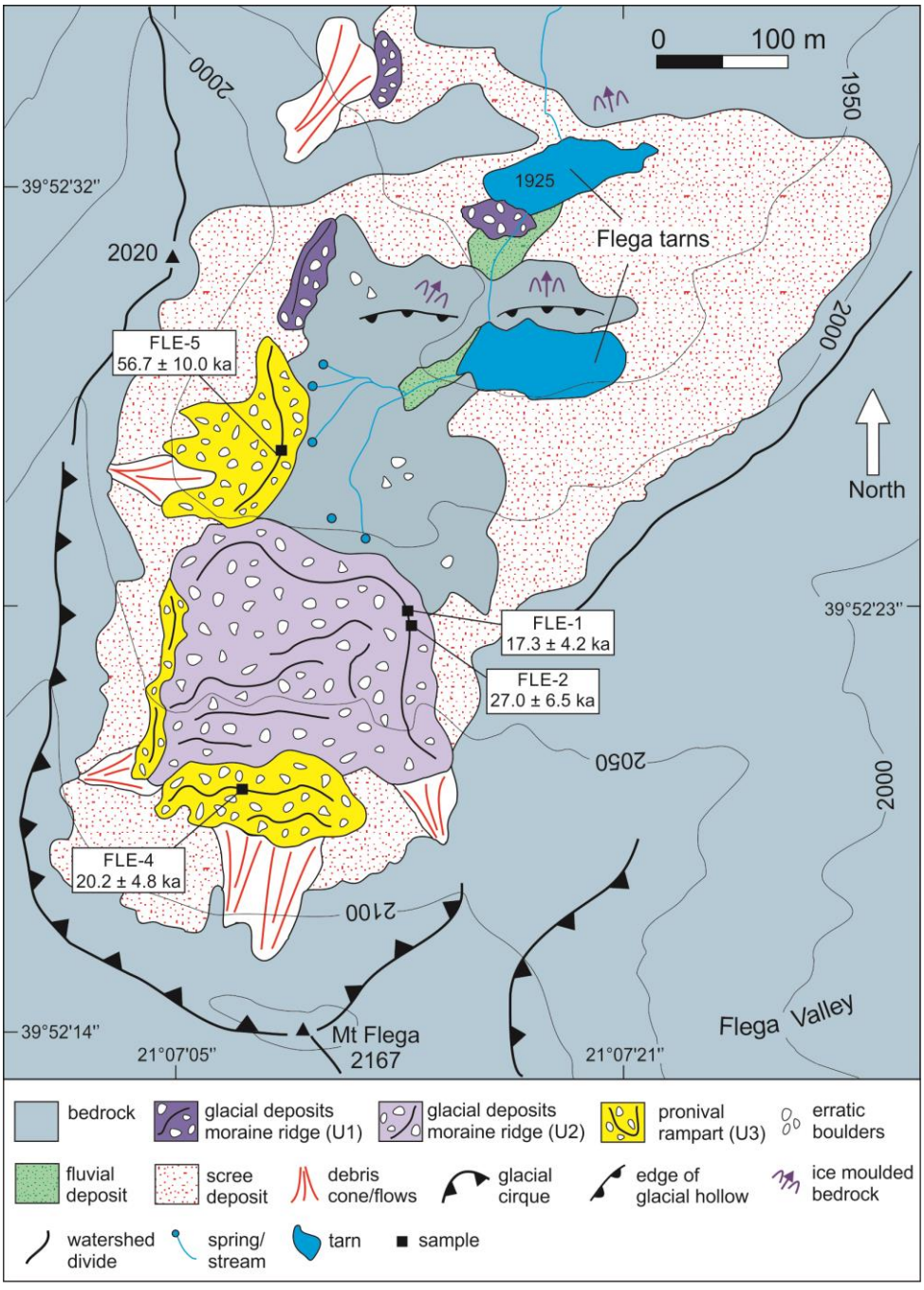

*Figure 6. Detailed glacial geomorphological map of the Mnimata Valley. This is panel B in Figure 1.*

The middle part of the valley, extending between 2000m a.s.l. and the treeline at 1850m a.s.l. is characterised by two tarns known as the Flega lakes and is dotted with erratic boulders (Figure 6, Figure 7a). Along the western flank of the valley, detrital ridges at the base of the slope were observed. The landform (evident crest slight sinuous or with an upvalley facing concavity) and the deposit characteristics are pretty similar to those of the pronival rampart sampled in the upper part of the valley. Therefore, these ridges have been ascribed to the same morphostratigraphic unit (Unit 3 in Table 3, Figure 4 and Figure 6). A single sample for $^{36}$Cl dating has been taken from one of the crests of these deposits at 1980 m a.s.l. (FLE-5 in Figure 5b and Figure 7b). Behind the crest there is angular debris that was most probably deposited after the disappearance of the nevé field according to mass wasting phenomena.


*Figure 7. a) (Top): Glacially transported and sub-rounded boulders between the two tarns; b) (Bottom): The Mnimata Unit 3 pronival rampart deposits at the W flank of the valley. Photo location shown in Figure 5b. Sample FLE-5 location is also denoted. Notice the streams nourishing the upper Flega tarn that spring below the deposits and onto the ice-scoured exposed impermeable bedrock that also hosts the two tarns (Photos August 2016).*

The two lakes are glacial in origin (Unit 1 in Table 3) but are not moraine-dammed as initially expected from the analysis of satellite imagery. In fact, they sit on ice scoured hollows on bedrock (Figure 7a). There are at least five springs just above the upper tarn where the aquifer meets the exposed impermeable bedrock (Figure 6, Figure 7b) and these springs nourish the two tarns. Between the tarns there are scattered glacial boulders (Figure 7a) whereas a pair of lateral moraines has been preserved on the western flank of the valley between 1900 and 2050m a.s.l. indicating the presence of a significantly larger palaeoglacier compared to the palaeoglacier corresponding to morphostratigraphic Unit 2(Figure 6). Ice-scoured and polished bedrock has been identified just below the lower tarn at 1900m a.s.l. that still bears clear striations in the direction of the paleaoglacier ice-flow on its surface (Figure 3), indicative of low postglacial erosion rates of the rock surface (Gosse and Philips, 2001). It should be noted that these features do not represent the lowermost depositional

limits of Unit 1 in this valley but rather mark the lower limit of valley accessibility and thus of the conducted fieldwork. Therefore, the correlation with the lowermost glacial deposits in the Flega and Arkoudolakos valleys (see Table 3) has been based on their relative stratigraphic position, palaeoglacier size and erosion extent of the recorded sediments.

### 4.1.2 Flega Valley

The Flega glacial valley has a N-NE orientation. Along its main axis runs the homonymous Flega stream which has caused deep cut-off erosion creating a steep, V-shaped bank-riverbed profile. The head of the valley is ice steepened, forming a wide and quite well-developed cirque. The edges of this cirque stand between 1950 and 2050m a.s.l. Glacial evidence in the upper valley is limited to scattered sub-rounded glacial boulders with quite indistinct depositional limits. However, a small moraine damming a swamp/seasonal lake (Figure 8) is present at an altitude of 1880m a.s.l. on the eastern flank of the valley. It has been correlated with Unit 2 deposits in the Mnimata valley on grounds of altitude and superficial form and has therefore been ascribed to morphostratigraphic Unit 2 (Table 3, Figure 4).


*Figure 8. a) (Top): The Flega Unit 2 moraine which dams a seasonal lake/swamp on the eastern part of the upper Flega valley; b) (Bottom): Glacially transported boulder outstanding on the glacial deposits damming the seasonal lake/swamp at the upper Flega valley. Notice the cracks in the boulder that upon further glacial working or freeze-thaw processes could have comminuted this 1.5m in diameter boulder into smaller clasts. (Photo: July 2018)*


*Figure 9. The inner flank of the Flega Unit 1 moraine (Photo: July 2018).*


382 *Figure 10. The Flega Unit 1 moraine; a) (top left): unsorted clast-supported deposits with a fine*
383 *gravel matrix and sandy to silty material at the lowermost part of the exposure; b) (top right):*
384 *subrounded clasts of variable size, from a diameter of 25cm to centimetric gravel; c (bottom): larger*
385 *subrounded and striated glacial boulders along the moraine crest (Photo: July 2018).*

In the lower part of the valley (below 1900m a.s.l.), a continuous lateral moraine extending from 1740 to 1840m a.s.l. in altitude and 600m in length has been classified into Unit 1 on the grounds of former glacial extent, signs of exhumation and relative stratigraphic position (Table 3, Figure 4, Figure 9, Figure 10). The moraine converges to the modern river channel, possibly indicating the position of the former glacier's snout, although the terminal frontal moraine must have been eroded from run-off water. This moraine has most probably been formed by a glacier originating from the central-western part of the NE Flega main cirque and the NE Flega sub-cirque, although an origin from the western section of the cirque cannot be excluded.

These ophiolite-dominated glacial sediments appear to be clast-supported, with prevalently ophiolitic clasts partly cemented by a scarce sandy to silty matrix (Figure 10a and b). The clasts are striated and subrounded. Larger boulders do not exceed 1.5m in diameter and are mostly evident along the moraine crest (Figure 10c). Contrary to moraines of granite/gneiss or limestone lithologies, no large blocks (>5m in diameter) are present in this ophiolite-dominated sedimentary unit due to the cracks and joints caused by structural deformation of the parent bedrock (e.g. Figure 8). These characteristics are consistent with Middle Pleistocene glacial deposits of ophiolitic lithology from Mt Smolikas (Hughes et al., 2006c) and Mt Vasilitsa (Hughes, 2004) (Figure 1).

#### 4.1.3 Arkoudolakos valley

The upper part of the Arkoudolakos glacial valley includes two converging valleys (Figure 4). The western branch has a NE orientation and is quite steep and inaccessible, thus it was excluded from field work. The N-oriented eastern branch is a U-shaped and wide valley but its head is smooth and does not bear typical glacial geomorphological features like a cirque or ice-steepened headwalls. However, scattered glacial boulders and remnants of sub-glacial till are evident throughout this valley branch (Figure 4). Similarly to the Flega

valley, the depositional limits are indistinct and, although these deposits could be correlated on terms of altitude with morphostratigraphic Unit 2 deposits from the two adjacent valleys, they could also very well be synchronous to the older and more extensive deposits lower in the valley that belong to morphostratigraphic Unit 1 (Figure 4).

The lower Arkoudolakos valley (part below the converging point of the two upper branches) has a N orientation (Figure 4), is densely forested and along its central axis has undergone V-shaped erosion by run-off water, which is typical for ophiolites (Hughes et al., 2006d). Two moraines have been identified in the lower part of the main valley forming the Bear Unit 1 moraines (Table 3). The first is a clear and well-shaped lateral moraine that extends right from the point where the two upper branches of the valley converge at 1660 m. a.s.l. and down to 1500m a.s.l. (Figure 4) where it has been washed away by the river that runs along the valley (Figure 11). Its total length is about 800 m. The second moraine is poorly preserved, extends from 1510 to 1470m a.s.l., and is 300m long. Both moraines are covered by dense beech forests and thus are unrecognisable from satellite imagery. No exposure of the moraines were discovered. The Bear Unit 1 moraines are correlated with the Flega Unit 1 moraine in the Flega valley on terms of altitude, stratigraphic position and signs of erosion (Figure 4)


*Figure 11. The Bear Unit 1 moraine; a) (up left): large glacial boulder (d~2 m) along the densely forested moraine b) (up right): subrounded and striated boulders and clasts along the well-shaped moraine crest and; c (below): another glacially transported large boulder next to the path that runs along the moraine ridge (backpack length ~0.6m for scale).*

## 4.2 Geochemistry

The geochemistry of the samples is presented in Table 4. All analyses were conducted by the Acme labs in Canada (Bureau Veritas Mineral Laboratories). Bulk rock compositions refer to the sample prior to any etching or cleanup, while the target rock sample represents the final, clean mineral fraction that was dissolved for AMS analysis. Bulk rock compositions are used to calculate neutron-transport parameters, which are particularly important for samples with significant production from neutron capture (see Marrero et al., 2016b).

*Table 4. Geochemistry of the serpentinized peridotite samples for $^{36}Cl$ dating. For major and minor elements, results are given for both bulk rock and target (processed) rock samples. (* ICP-ES, **ICP-MS, ***$LiBO_2/Li_2B_4O_7$ fusion & ICP-ES)*

| Major and minor element mass fraction (wt %) |
|---|

| Sample ID | $SiO_2$ | $Al_2O_3$ | $Fe_2O_3$ | MgO | CaO | $Na_2O$ | $K_2O$ | $TiO_2$ | MnO | Water (LOI) | $CO_2$ |
|---|---|---|---|---|---|---|---|---|---|---|---|
| Bulk rock samples* | | | | | | | | | | | |
| FLE-1 | 43.44 | 0.43 | 8.21 | 41.22 | 0.36 | 0.02 | 0.01 | <0.01 | 0.11 | 4.6 | 0.6 |
| FLE-2 | 44.17 | 0.22 | 8.48 | 42.33 | 0.24 | 0.01 | <0.01 | <0.01 | 0.12 | 2.9 | 0.6 |
| FLE-4 | 41.48 | 0.21 | 8.35 | 40.38 | 0.21 | 0.01 | <0.01 | <0.01 | 0.11 | 7.5 | 0.6 |
| FLE-5 | 45.03 | 1.61 | 8.35 | 39.45 | 1.42 | 0.03 | <0.01 | 0.02 | 0.12 | 2.5 | 0.6 |
| Target rock samples** | | | | | | | | | | | |
| FLE-1 | 45.98 | 0.43 | 8.63 | 39.36 | 0.39 | 0.01 | <0.01 | <0.01 | 0.11 | - | - |
| FLE-2 | 46.3 | 0.22 | 8.88 | 41.26 | 0.24 | <0.01 | <0.01 | <0.01 | 0.12 | - | - |
| FLE-4 | 44.16 | 0.24 | 8.58 | 39.16 | 0.2 | <0.01 | <0.01 | <0.01 | 0.1 | - | - |
| FLE-5 | 46.21 | 1.8 | 8.64 | 38.62 | 1.61 | 0.03 | <0.01 | 0.02 | 0.12 | - | - |

Trace element concentrations (ppm)

| Sample ID | B | Sm | Gd | U | Th | Li | V | Ba | Ni | Sc | Co |
|---|---|---|---|---|---|---|---|---|---|---|---|
| Bulk rock*** | | | | | | | | | | | |
| FLE-1 | <3 | <0.05 | <0.05 | <0.1 | <0.2 | <0.001 | 22 | 8 | 2388 | 6 | 123.6 |
| FLE-2 | <3 | <0.05 | <0.05 | <0.1 | <0.2 | <0.001 | 16 | 10 | 2473 | 5 | 126.5 |
| FLE-4 | <3 | <0.05 | <0.05 | <0.1 | <0.2 | <0.001 | 23 | 4 | 2470 | 4 | 123.6 |
| FLE-5 | <3 | <0.05 | 0.06 | <0.1 | <0.2 | <0.001 | 51 | 6 | 2214 | 11 | 113.3 |

Bulk rock compositions primarily reflect the proportions of minerals present. Based on these compositions, these rock samples are peridotites/harzburgites with predominant serpentine alteration (Dilek et al., 1997a; Kelemen et al., 2004). A rock density of 2.7 g $cm^{-3}$ was considered for all samples (Table 1), in accordance to the respective values for ultramafic peridotites with medium to high serpentinization degree (>70%) from the Pindus ophiolitic complex (Bonnemains et al., 2016). XRD analyses of highly serpentinized ultramafic rocks from oceanic crust in the Mid-Atlantic Ridge showed that Loss On Ignition (LOI) can be attributed entirely to water content (Kelemen et al., 2004) whereas an average value for $CO_2$ concentrations is 0.6 wt% (Kelemen et al., 2011). It is noted that the slight

underestimation of the total volatile content is caused by the conversion of FeO to $Fe_2O_3$ during heating of the sample powders for LOI estimation (Kelemen et al., 2004). This approach was adopted in this paper, attributing the measured LOI entirely to water content and assuming a 0.6 wt% of $CO_2$ concentration for all samples (Table 4).

### 4.3 $^{36}$Cl exposure ages

The two samples FLE-1 and FLE-2 were taken from the largest (up to 1m diameter) and most stable boulders which were partly embedded along the ridge of a well-consolidated terminal moraine (Figure 12a) reducing the possibility of dating inaccuracies due to post depositional processes such as moraine dismantling and boulders toppling . FLE-1 and FLE-2 yielded $^{36}$Cl exposure ages of 17.3 ± 4.2 ka and 27.0 ± 6.5 ka, respectively.

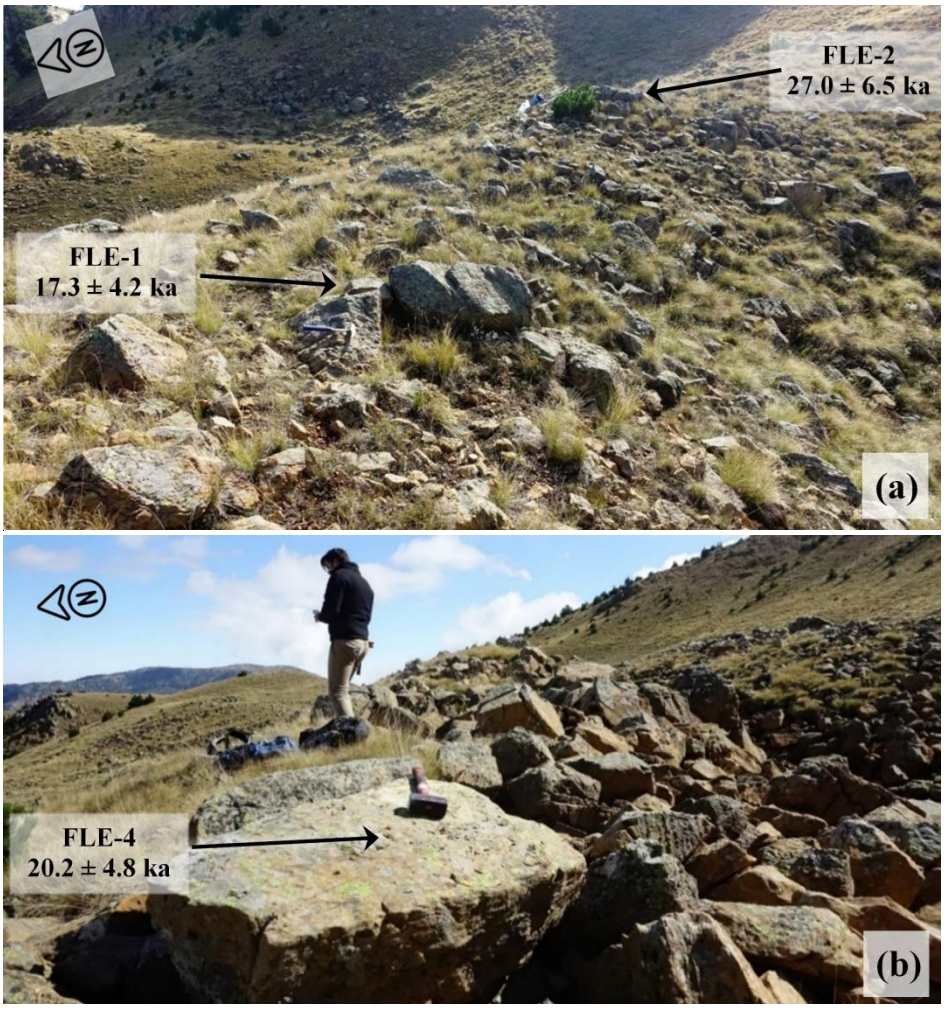

*Figure 12. a) (Top):Sampled boulder on the well-consolidated terminal moraine (samples FLE-1 &FLE -2); b) (Bottom): Sampled boulder on the crest of the less-consolidated pronival deposits (sample FLE-4). Exact samples locations are given in Figures 5 and 6. (Photos: October 2016)*

Further upvalley, pronival deposits are less consolidated than the morainic deposits and are typically characterised by larger (1-5m diameter) and more angular boulders and the absence of a matrix consisting of gravels and fines (Hedding and Sumner, 2013). Two stable boulders along the most consolidated part of the pronival deposits were chosen for sampling (FLE-4 and FLE-5, Figure 12b). The $^{36}$Cl exposure ages for these two samples were calculated at 20.2 ± 4.8 ka and 56.7 ± 10.0 ka respectively.

The apparent exposure ages of the four samples as well as the respective elemental contribution to total $^{36}$Cl production as calculated with the CRONUScalc $^{36}$Cl Exposure Age Calculator v2.2 are summarised in Table 5. All ages are within the Late Pleistocene as initially expected but most importantly samples FLE-2, FLE-4 and FLE-5 fall in the LGM interval within the respective uncertainties.

*Table 5. Exposure ages, share of total $^{36}$Cl production per element as calculated with CRONUScalc $^{36}$Cl Exposure Age Calculator v2.2 for the considered samples. Uncertainties include analytical and production rate uncertainties. Reported percentages of $^{36}$Cl production correspond to production from spallation and slow muons for Ca and K, low energy neutrons for Cl and spallation only for Fe and Ti.*

| *Results obtained with CRONUScalc $^{36}$Cl Exposure Age Calculator v2.2* | | | | | | |
|---|---|---|---|---|---|---|
| Sample ID | Age (ka) | Percentage of total $^{36}$Cl production (%) | | | | |
| | | Cl | Ca | K | Fe | Ti |
| FLE-1 | 17.3 ± 4.2 | 88.23 | 6.11 | 0 | 5.65 | 0 |
| FLE-2 | 27.0 ± 6.5 | 91.02 | 3.52 | 0 | 5.45 | 0 |
| FLE-4 | 20.2 ± 4.8 | 96.97 | 1.08 | 0 | 1.95 | 0 |

| | | | | | | |
|---|---|---|---|---|---|---|
| FLE-5 | 56.7 ± 10.0 | 56.94 | 35.22 | 0 | 7.80 | 0.04 |

485

### 4.3.1 Implications of iron-rich ophiolitic lithologies on cosmogenic $^{36}$Cl exposure dating

488 The glacial chronology of Mt Mavrovouni relies on the application of cosmogenic $^{36}$Cl
489 surface exposure dating on highly serpentinized ophiolites. In this study, due to low Ca and K
490 concentrations, the cosmogenic $^{36}$Cl has been mainly produced from Cl with a non-negligible
491 contribution from Fe (Table 5), making these production rates more important than in
492 samples of other lithologies. The relatively high uncertainties of the calculated ages are a
493 result of the domination of $^{36}$Cl production from the capture of thermal neutrons by $^{35}$Cl in
494 the rock and the higher uncertainty associated with the production from this pathway
495 (Marrero et al, 2016a; Asimov and Ivy-Ochs, 2009).

496 The Fe pathway accounts for ~2-8% of the total $^{36}$Cl production (Table 5), which is much
497 higher than the 1-2% combined Ti and Fe contributions in most common rock types (Marrero
498 et al., 2016a), so it has not been included as a calibrated parameter in recent calibrations (e.g.
499 Schimmelpfennig et al., 2009; 2011; Marrero et al., 2016a ). In our case, the rock samples are
500 characterised by high concentrations of $Fe_2O_3$ (8-8.5%) (Table 4). As the current version of
501 the CRONUScalc online calculator (v2.1;
502 http://cronus.cosmogenicnuclides.rocks/2.1/html/cl/; Marrero et al., 2006b) has not been
503 specifically calibrated for production rates from Fe spallation, significant production from Fe
504 was investigated further here. The exposure ages of the samples were recalculated using a
505 modified version of the original CRONUScalc code (v2.2, available on
506 https://bitbucket.org/cronusearth/cronus-calc/; accessed 15 Sept 2021). In this version, new
507 Fe production rates of 1.29 ± 0.11 atoms $^{36}$Cl (g Fe)$^{-1}$ yr$^{-1}$ as reported from Moore and
508 Granger (2019) are incorporated into CRONUScalc and used in conjunction with the LSDn
509 scaling model as described in Anjar et al. (2021). This required recalibrating the main $^{36}$Cl

production rates, resulting in <1% change in the production rates for the main pathways (Anjar et al., 2021) when compared to the previous production rates (Marrero et al., 2016a; 2021). The results obtained show negligible differences (<1%) in the resulting ages compared with the results obtained with the latest online version (v2.1) of the calculator. Moore and Granger (2019) underline that additional data are needed to confirm the scaling behaviour described in their work, so high-Fe samples like these could be used to contribute towards this effort.

# 5 Discussion

## 5.1 Glacial chronology and interpretation

Sampling was limited to the stratigraphically youngest set of glacial deposits in the Mnimata valley (Figure 6). The sampling strategy was dictated by the aim to establish a preliminary chronology of this glacial/periglacial sequence and confirm that its formation falls within the LGM as suggested by morphostratigraphic correlations of moraines within the Pindus mountains (Mt Tymphi, Mt Smolikas and Mt Mavrovouni; Figure 1). However, the small number of ages and the high level of uncertainty in the calculated ages means that additional data are needed in order to establish a tighter and reliable chronology of cold events on Mt Mavrovouni. Next, a preliminary chronology according to the obtained $^{36}$Cl surface exposure ages is presented.

The $^{36}$Cl exposure ages for the main terminal moraine samples FLE-1 and FLE-2 (Unit 2 in Table 3, Figure 4 and Figure 6) were 17.3 ± 4.2 ka and 27.0 ± 6.5 ka, respectively (Table 5). The older age is considered to be the most representative for moraine deposition whilst the younger one may represent a period of boulder toppling or exhumation (Ivy-Ochs et al., 2006a, 2006b, 2007; Ivy-Ochs and Kober, 2008; Ivy-Ochs and Briner, 2014). This is because sample FLE-1 (which yielded the younger age) was taken from the proximal (inner) side of the moraine which is more susceptible to degradation and mass wasting processes. FLE-2

(which yielded the older age) was taken from one of the highest points on the moraine ridge making it less likely to have undergone significant toppling or exhumation (Ivy-Ochs et al., 2006a, 2006b, 2007). Assuming the mean of the two ages as landform age was not considered as it is susceptible to significant inaccuracies (Ivy-Ochs et al., 2007), especially if incomplete exposure and moraine dismantling are suspected (Applegate et al., 2010; D'Arcy et al., 2019). Thus, in this preliminary chronology this moraine is considered to have been formed by an advancing cirque glacier when it reached its maximum extent close in time to the global LGM interval (27.5-23.3 ka; Hughes and Gibbard, 2015) as the age of sample FLE-2 falls within this interval but additional data is in any case needed to strengthen this chronology. This age also provides the maximum age of formation of Unit 2glacial deposits on Mt Mavrovouni which falls close to the LGM interval within the calculated age uncertainties.

As the geomorphological evidence (terminal moraine and cirque walls) define sufficiently the limits of this palaeoglacier it was possible to use a geographical information systems approach (GIS) to calculate its palaeo-ELA at 2090m above modern sea level. In particular, the surface, thickness and ELA of the former glaciers were reconstructed using the semi-automated GIS tools based on the numerical technique of Benn and Hulton (2010) and developed by Pellitero et al. (2015; 2016). The ELA was calculated with the adaptation of the classic area– altitude balance ratio (AABR) method (Osmaston, 2005) using a balance ratio (BR) of 1.6, which is the average obtained on present-day glaciers in other Mediterranean mountains (Rea, 2009).

The stratigraphically youngest deposits within the Mnimata sequence (Unit 3 in Table 3, Figure 4 and Figure 6) are interpreted as relict pronival ramparts. More importantly, their preliminary age of deposition discussed here marks a cold period with persistent snow/ice cover or permafrost occurrence whilst at the same time constitutes the lower limit for the

timing of deposition of the Mnimata sequence. The uppermost part of this set of deposits (FLE-4) and that at the western flank of the upper valley (FLE-5) were expected to have formed synchronously regardless of their different altitude as they belong to two morphologically and compositionally similar ridges expanding along the W-E and S-N axes respectively and both have been deposited directly below the slopes above them. However, the samples yielded ages of 20.2 ± 4.8 ka and 56.7 ± 10.0 ka respectively. The most representative age for the formation of these features is considered to be the younger one as the pronival ramparts in question are stratigraphically younger than the terminal moraine ridge that was dated at 27.0 ± 6.5 ka. Moreover, the FLE-4 sample was taken from a large and well stabilised boulder on the highest point of the pronival rampart within a section of angular deposits lacking finer material and therefore minimising the probability of exhumation or other mass wasting processes (Allard et al., 2020). On the other hand, the FLE-5 age could have been affected by inheritance of $^{36}$Cl atoms from previous exposure. However, marked inheritance in moraine boulders (and similarly in pronival ramparts) is rare (Heyman et al., 2011) and incomplete exposure is more likely to be an issue (Ivy-Ochs and Briner, 2014). Therefore, a more probable interpretation is that the morphology of this sedimentary unit is composite. It is likely that an older lateral moraine associated with the stratigraphically older Unit 1 pre-LGM deposits was later partly overlapped by a nested pronival rampart. In this case, the moraine itself became, once the glacier had disappeared, a starting ridge at the base of the slope which then evolved into a pronival rampart. The age of this sample could then represent a period of boulder exhumation. Additional dating data are also needed in this case to support this preliminary chronology. The deposition age of Unit 3 sediments are is thus here considered at20.2 ± 4.8 ka, probably within the LGM interval but with a considerable level of uncertainty as the respective age range indicates.

584 The most extensive glaciation phase is represented by a single morphostratigraphic unit
585 (Unit 1 in Table 3, Figure 4 and Figure 6). This unit may represent more than one phase of
586 glaciation, possibly widely separated in time, but it was not possible to distinguish multiple
587 moraine units that correspond to different glacial stages, possibly widely separated in time,
588 but it was not possible to distinguish multiple moraine units that correspond to different
589 glacial stages. Nevertheless it is clearly distinguished from Units 2 and 3 as these
590 stratigraphically older moraines are at lower altitudes and show considerably more signs of
591 erosion and higher level of soil development. These moraines remain undated but, on the
592 basis of morphostratigraphic correlations (relative stratigraphic position, elevation, erosion
593 and soil development) with the moraines in the nearby Mt Tymphi (Woodward et al., 2004;
594 Hughes et al., 2006a) as well as in Mt Chelmos in southern Greece (Pope et al., 2017; Figure
595 1) and in the mountains of Montenegro (Hughes et al. 2010, 2011), they are likely Middle
596 Pleistocene in age. Particularly, this glacial phase may correspond to the Skamnellian
597 (MIS12) and/or the Vlasian Stage (MIS6) of northern Greece.

598 **5.2 The Glacial history of the Pindus Mountains and Greece in a regional context**

599 **5.2.1 Pre-LGM Pleistocene glaciations**

600 The most extensive glacial phases in the mountains of Greece most probably took place
601 during Middle Pleistocene and particularly during MIS 12 (Skamnellian Stage) and MIS 6
602 (Vlasian Stage). This was established by the studies on Mt Tymphi (Woodward et al., 2004;
603 Hughes, 2004; Hughes et al., 2006a) and in the mountains of Montenegro (Hughes et al.,
604 2010, 2011) based on maximum U-series ages from secondary calcites present in limestone-
605 derived moraines/till. It should be noted that the ages of the Skamnellian Stage moraines are
606 beyond the upper limit of U-series dating which is 350 ka (Woodward et al., 2004; Hughes et al.,
607 2006a). It is important to recognise that as U/Th ages denote the age of secondary calcites
608 formation sometime after deposition and in this case during the more favourable warm

609 interglacial periods, the oldest ages for a particular deposit can be used to infer glacial activity
610 during a previous cold stage (Woodward et al., 2004). For this reason, the ages from the older
611 moraines (>350 ka) indicate that calcites formation was associated with MIS 11 (or older)
612 although the precise ages are unknown (Woodward et al., 2004; Hughes et al., 2006a). Taking
613 also into account that the next glacial period preceding 350ka (MIS 11) is MIS 12 which is
614 considered to be the most extreme climatic glacial interval of the last ~500 ka (Tzedakis et al.,
615 2003) the deposition of these moraines was ascribed to this interval (Hughes et al., 2006a).

616 This chronology could potentially be independently tested with the application of $^{36}$Cl
617 surface exposure dating to the ice-scoured bedrock recorded below the twin tarns in the
618 Mnimata valley in order to constrain the timing of the most extensive glacial phase on Mt
619 Mavrovouni (Unit 1 in Table 3; Figure 3). However, it is likely that exposure dating on such
620 old surfaces may yield just minimum ages due to surface erosion, although it should be a
621 target for future research.

622 **5.2.2 Glaciations during the global LGM**

623 The LGM $^{36}$Cl dates presented in this paper from ophiolite-derived moraines on Mt
624 Mavrovouni are consistent with the $^{36}$Cl dates from limestone moraines on the nearby Mt
625 Tymphi (Allard et al., 2020), suggesting a Late Pleistocene local glacial maximum close in
626 timing to the global LGM interval (27.5-23.3 ka) within the errors of the calculated ages. In
627 particular, the largest Late-Pleistocene glaciers on Mt Tymphi reached their terminal
628 positions no later than 25.7 ± 2.6 - 29.0 ± 3.0 ka and had an ELA of 2016m a.s.l. (Allard et al.,
629 2020). Glaciers had retreated to the high cirques by 24.5 ± 2.4 ka (Allard et al., 2020) during
630 Heinrich Stadial 2 (HS2: 26.5 -24.3 ka; Sanchez Goñi and Harrison, 2010). This timing of a
631 near-LGM late Pleistocene glacier maximum is confirmed by the $^{36}$Cl geochronology of
632 ophiolitic glacial boulders from a terminal moraine on Mt Mavrovouni presented here,
633 indicating stabilisation of the most extensive Late Pleistocene glaciers at 27.0 ± 6.5 ka. On

nearby Mt Smolikas (Figure 1), the well-formed moraines at 2000-2200m a.s.l., which have been ascribed to the last cold stage (MIS5d-2) but remain undated (Hughes et al., 2006d), may also be attributed to a glacial advance phase prior to, or within, the LGM.

The timing constraint of a local Late Pleistocene glacial maximum in the Pindus mountains in northwest Greece during the LGM interval is in good agreement with well-preserved outwash sediments dating to 28.2 ± 7.0 - 24.3 ± 2.6 ka (U-series; ESR, TL ages; Lewin et al., 1991; Hamlin et al., 2000; Macklin and Woodward, 2009 and references therein) in the Voidomatis River catchment which drains the southern part of Mt Tymphi including extensively glaciated slopes . This is also consistent with the Ioannina basin pollen record about 30km southwest from Mt Mavrovouni (Tzedakis et al., 2002; Figure 1), indicating cool and wet conditions, most favourable for glacier growth, at 30-25 ka (see discussion in Allard et al., 2020). The late half of the LGM interval (25.5 - 23.3 ka) is less favourable for a local glacial maximum despite coinciding with climatic deterioration during HS2 and a marked regional temperature depression between 25.6 and 23.2 ka (Macklin et al., 1997; Galanidou et al., 2000; Hughes, 2004). This is because cold and drier conditions reduced regional moisture supply inhibiting glacial growth (see discussion in Allard et al., 2020).

In the Peloponnese in southern Greece, Pope et al. (2017) showed that Late Pleistocene glaciers on Mt Chelmos (Figure 1) reached their maximum extent at 36.5 ± 0.9 - 28.6 ± 0.6 ka with a mean ELA of 2046 m a.s.l. (Pope et al., 2017 -recalculated ages by Allard et al., 2020) suggesting that glaciers from MIS 3 to 2 in the cirques of Mount Chelmos are likely to have oscillated with varying climatic conditions, especially in response to millennial-scale shifts between cold/dry and cool/wet conditions in Greece (Leontaritis et al., 2020; see also discussion in Hughes et al., 2006c). The results here (27.0 ± 6.5 ka) cannot be used to rule out a pre-LGM advance within the Late Pleistocene, taken into consideration that this age is more

likely to represent a minimum age of exposure after the glacier had retreated from the moraine (and especially given the assumption of negligible erosion in the age calculation). However, given the limited sample size and although the presented chronology is well supported by local and regional morphostratigraphic correlations, more data is needed to build a more robust age model.

As regards the calculated ELAs of LGM palaeoglaciers across Greece a crucial issue when attempting comparisons is the consideration of the tectonic uplift history of the different massifs (Giraudi and Giaccio, 2015). The North Pindus mountains are characterised by estimated tectonic uplift rates of 0.4–0.8 mm/yr corresponding to a total uplift of 10-20m for the last 25ka although rates might be higher (King and Bailey, 1985). These roughly estimated rates regard a wide area (>9000 $km^2$) with many local faults in the numerous massifs and include significant uncertainties. (Leontaritis, 2021). It is therefore likely that uplift rates may vary for each mountain area and especially between the limestone-dominated Mt Tymphi and the ophiolitic Mt Mavrovouni. Thus, any conclusions derived from ELA comparisons between these massifs may be problematic. Tectonic movements are even more active in the northern Peloponnesus area, where uplift rates have been estimated at 1.1-1.3 mm/yr over the last 350-500ka corresponding to a total uplift of 37-40m for the last 25ka (Armijo et al.,1996; De Martini et al., 2004; McNeill and Collier, 2004).

The first estimates of ELAs of LGM palaeoglaciers on Mt Mavrovouni (2090m a.s.l.), Mt Tymphi (~2000m a.s.l.) and Mt Chelmos (~2010m a.s.l.) indicate that glaciers during the LGM may have formed under similar climatic conditions across Greece. However, given the uncertainties in the uplift history of these mountains this conclusion should be considered with caution.

A pre-LGM local Late Pleistocene glacier maximum is evidenced in other Mediterranean mountains (Leontaritis et al., 2020). In particular, similar pre-LGM glacier advance phases

have been recorded in the Italian Apennines (33-27 ka; Giraudi, 2012; Giraudi and Giaccio, 2015 and references therein), the Pyrenees (García-Ruiz et al., 2010), the Segundera and Cabrera mountain ranges in northern Spain (33 ka; Rodriguez-Rodriguez et al., 2011), the Sierra Nevada in southern Spain (30-35 ka; Gómez-Ortiz et al., 2012; Palacios et al., 2016) and the western and central Taurus Range in Turkey [35 ± 2.5 - 28.1 ± 2.6 ka on Mt Akdağ (Sarıkaya et al., 2014); 46.0 ± 7 - 29.8 ± 2.3 ka on Mount Bolkar (Çiner and Sarıkaya, 2017); 29.7 ± 2.9 ka on the Dedegöl Mountains (Köse et al., 2019). Glacial advance during MIS3/early MIS2 in these areas has been associated with the prevalence of optimal cold and wet conditions (Oliva et al., 2019).

### 5.2.3 After the global LGM

At a global level, the LGM is succeeded by an interval associated with changes on the northern summer insolation induced by orbital forcing that resulted in the onset of Termination I at high latitudes and mountain regions at 19–20 ka, as well as an abrupt rise in sea level (Clark et al., 2009; Shakun et al., 2015). On Mt Mavrovouni in Greece, the presented evidence from periglacial features (Unit 3 in Table 3; FLE-4 in Table 5 and section 5.1) suggests that after the LGM, cold conditions persisted until 20.2 ± 4.8 ka but were unable to sustain dynamic glaciers. The deposition of pronival ramparts has been associated with the presence of perennial snow/nevé fields within the topographically shaded glacial cirque slopes and the increased debris supply due to freeze-thaw weathering of the cirque walls. Furthermore, on Mt Tymphi, initial results suggest that small glaciers (<0.6 $km^2$) persisted only in the topographically shaded northeast cirques up until 18.0 ± 1.9 ka, (Allard et al., 2020). The presence of rock glaciers below these small cirque glaciers, which are stratigraphically younger than the cirque moraines formed at 25.7 ± 2.6 ka (Allard et al., 2020), has been interpreted as the result of arid and cold climate conditions in the interval 25-20 ka (Hughes et al., 2003). The evidence from Mt Mavrovouni and Mt Tymphi thus suggests

unfavourable (cold and arid) conditions for glacier development during this transitional phase from the LGM to the Late-glacial but cold/humid enough to preserve perennial snow fields (i.e. nevé fields), permafrost and rock glaciers as well as small glaciers in topographically favourable positions. This is consistent with other proxies derived from Lake Ioannina – approximately 30 km south of Mt Tymphi and Mt Mavrovouni (Figure 1) – which indicate locally cold and drier climate persisting during this period that would have inhibited glacier development (see discussion in Allard et al., 2020), such as low lake levels between 22 and 20 ka (Frogley, 1998) and a drop of temperatures by 7-10$^{o}$C with annual rainfall around 600 mm as it has been estimated by the analysis of the lacustrine pollen record (Tzedakis et al., 2002). Finally, a decline in limestone-derived fine sediment input from 24.3 ± 2.6 to 19.6 ± 3.0 ka (U-series ages) in the Voidomatis River record implies shrinking glaciers in its headwaters in the south-facing cirques of Mt Tymphi compared to the earlier part of the LGM (Macklin et al., 1997). The younger age limit is consistent with unfavourable conditions for glacial growth and the deposition of pronival ramparts on Mt Mavrovouni and overlaps within uncertainty with a possible moraine deposition in the northeast cirques of Mt Tymphi discussed above, thus giving some support to this initial evidence for small glaciers/neves in the 20-18 ka interval (Allard et al., 2020). Nonetheless, more data are needed from this period in the Pindus Mountains in order to build a more robust age model.

#### 5.2.4 The Pindus Mountains: a summary

The recently produced geochronological data for the Last Glacial Cycle (MIS 5d-2) in the mountains of Greece have proved crucial for addressing the most important temporal gap in the geochronology of the glacial history of Greece (Leontaritis et al., 2020). The Late Pleistocene $^{36}$Cl surface exposure ages have been carefully examined in the current glacial framework of the Pindus Mountains following recommended approach of Ivy-Ochs and Kober (2008). This includes geomoprhological field studies, local and regional

734 morphostratigraphic correlations (Palmentola et al., 1990; Boenzi et al., 1992; Woodward et
735 al., 2004; Hughes, 2004; Hughes et al., 2006a; 2006d; Allard et al., 2020) as well as
736 independent age constraints (U-series - Hughes et al., 2006a; $^{36}$Cl dating of limestone-
737 dominated moraines - Allard et al., 2020; $^{36}$Cl dating of ophiolite-dominated moraines - this
738 paper). However, although the Late Pleistocene glacial record of the Pindus mountains in
739 Greece is today one of the best-established and most accurately dated in the Balkans, the
740 existence and dynamics of glaciers in the Pindus mountains during the cold events of the
741 Late-glacial (17.5-11.7 ka; Rasmussen et al., 2006, 2014) remains poorly elucidated. Late-
742 glacial features in the Pindus mountains are absent both on Mt Mavrovouni and on Mt
743 Tymphi (Allard et al., 2020) and their presence seems to be limited to Mt Smolikas (Hughes
744 et al. 2006d; Leontaritis et al., 2020), where four discrete phases of Pleistocene glacial
745 activity are recognised (MIS12; MIS6; LGM and post-LGM; Hughes et al., 2006d). The Mt
746 Smolikas post-LGM glacial phase might correspond to the Younger Dryas (Hughes, 2004;
747 Hughes et al., 2006d). The glacial sequence on Mt Smolikas is the most complete recorded
748 glacial sequence in the Pindus mountains (Leontaritis et al., 2020) but its potential has only
749 been partially explored as its ophiolitic lithology has prevented (until now) the dating of its
750 moraines with absolute dating methods (Hughes et al., 2006a; Woodward and Hughes, 2011).
751 The applicability of the cosmogenic $^{36}$Cl surface exposure dating method to ophiolites
752 demonstrated here opens up the possibility of a future dating program on Mt Smolikas.

753 # 6 Conclusions

754 In addition to providing important new insights to the glacial geomorphology of the
755 Pindus Mountains this paper presents new surface exposure age results from a pilot study
756 using $^{36}$Cl to date ophiolite glacial boulders. Despite the small number of samples and
757 relatively large uncertainties, these ages confirm that the last glaciation on Mt Mavrovouni
758 occurred during the last glacial cycle and most probably during the LGM. Moreover they are

well supported by local and regional morphostatigraphical correlations and are consistent with $^{36}$Cl surface exposure ages from limestone-derived moraines on the nearby Mt Tymphi as well as the Voidomatis River record within the same massif and the Ioaninna basin pollen record. This study provides confidence in the suitability of $^{36}$Cl dating for iron-rich ophiolites using improved production rates from iron spallation, meaning that future studies can provide additional chronology for the highest peaks of the Pindus and the wider Balkans which are formed of a similar lithology.

The presented preliminary chronology was based on the geomorphological study, on the obtained ages as well as on the established morphostratigraphic correlations. At least three distinct Pleistocene cold phases were identified. Glaciers reached their local Late Pleistocene maximum within the global LGM interval at 27.0 ± 6.5 ka. Cold conditions persisted until 20.2 ± 4.8 ka when a combination of retreating glaciers, permanent snow fields, permafrost and increased debris supply due to freeze-thaw weathering of the cirque walls led to the formation of periglacial landforms such as rock glaciers and pronival ramparts. This evidence suggests unfavourable (cold and arid) conditions for glacier development during this transitional phase from the global LGM to the Late-glacial but cold/humid enough to preserve perennial snow fields (i.e. nevé fields) and small glaciers in topographically favourable positions supporting the hypothesis of increasing aridity prevailing across Western Balkans after the global LGM. The geomorphological and sedimentological evidence of a more extensive, pre-LGM glaciation phase(s) is also evident. This can be attributed to the Middle Pleistocene (MIS 12/MIS 6) on the basis of regional morphostratigraphic correlations.

**Acknowledgements**

We would like to thank Dr Costas Athanassas for his help in collecting and crushing the samples. We are also thankful to Dr. Pierre Valla and an anonymous reviewer for their constructive comments during the review process of this article.

## References


Allard, L.J., Hughes, P.D., Woodward, J.C., Fink, D., Simon, K., Wilcken, K.M. (2020). Late Pleistocene glaciers in Greece: A new $^{36}$Cl chronology. *Quaternary Science Reviews 245*, 1-27. https://doi.org/10.1016/j.quascirev.2020.106528

Anavasi (2016). Valia Kalda -Vasilitsa 1:50,000 hiking map [Topo 50, 6.4]. Anavasi Maps & Guides, Athens, Greece.

Anjar, J., Akçar, N., Larsen, E.A., Lyså, A., Marrero, S., Mozafari, N., Vockenhuber, C. (2021). Cosmogenic Exposure Dating ($^{36}$Cl) of Landforms on Jan Mayen, North Atlantic, and the Effects of Bedrock Formation Age Assumptions on $^{36}$Cl Ages. *Geosciences 11*, 390. https://doi.org/10.3390/geosciences11090390

Applegate, P.J., Urban, N.M., Laabs, B.J.C., Keller, K., Alley, R.B. (2010). Modeling the statistical distributions of cosmogenic exposure dates from moraines. *Geoscientific Model Development (GMD) 3*, 293-307. https://doi.org/10.5194/gmd-3-293-2010

Armijo, R., Meyer, B.G., King. G.P., Rigo, A., Papanastassiou, D. (1996). Quaternary evolution of the Corinth Rift and its implications for the Late Cenozoic evolution of the Aegean. *Geophysical Journal International 126*, 11-53. https://doi.org/10.1111/j.1365-246X.1996.tb05264.x

Asimov, V. And Ivy-Ochs, S. (2009). How well do we understand production of $^{36}$Cl in limestone and dolomite? *Quaternary Geochronology 4*, 462-474. https://doi.org/10.1016/j.quageo.2009.08.005

Bahr, D.B., Pfeffer, W.T., Sassolas, C. and Meier, M.F. (1998) Response time of glaciers as a function of size and mass balance:1. Theory. *Journal of Geophysical Research 103*, 9777-9782. https://doi.org/10.1029/98JB00507

Balco, G. and Schaeffer, J.M. (2006). Cosmogenic nuclide and varve chronologies for the deglaciation of southern New England. *Quaternary Geochronology 1*, 15-28. https://doi.org/10.1016/j.quageo.2006.06.014

Boenzi, F., Palmentola, G., Sanso, P. and Tromba, F. (1992). Le Tracce Glaciali Del Massiccio Dello Smolikas (Catena Del Pindo – Grecia). *Rivista Geografica Italiana 99*, 379-393.

Bourcart J. (1922). *Les Confins Albanais Administrés Par La France (1916-1920): Contribution a la Géographie Et a la Géologie de l'Albanie Moyenne*. Paris, France: Librairie Delagrave, pp. 104.

Benn, D.I. and Ballantyne, C.K. (2005). Palaeoclimatic reconstruction from Loch Lomond Readvance glaciers in the West Drumochter Hills, Scotland. *Journal of Quaternary Science 20*, 577–592. https://doi.org/10.1002/jqs.925

Benn, D.I. and Hulton, N.R.J. (2010). An Excel (TM) spreadsheet program for reconstructing the surface profile of former mountain glaciers and ice caps. *Computers and Geosciences 36*, 605–610. https://doi.org/10.1016/j.cageo.2009.09.016

Bonnemains, D., Carlut, J., Escartın, J., Mevel, C., Andreani, M., Debret, B. (2016). Magnetic signatures of serpentinization at ophiolite complexes. *Geochemistry Geophysics Geosystems 17*, 2969–2986. https://doi.org/10.1002/2016GC006321

Chadwick, O.A., Hall, R.D., Phillips, F.M. (1997). Chronology of glacial advances in the central Rocky Mountains. *Geological Society of America Bulletin 109*, 1443–52. https://doi.org/10.1130/0016-7606(1997)109<1443:COPGAI>2.3.CO;2

Chandler, B.M.P., Lovell, H., Boston, C.M., Lukas, S., Barr, I.D., Benediktsson, Í.Ö., Benn, D.I., Clark, C.D., Darvill, C.M., Evans, D.J.A., Ewertowski, M.W., Loibl, D., Margold, M., Otto,J.-C., Roberts, D.H., Stokes, C.R., Storrar, R.D., Stroeven, A.P. (2018). *Glacial geomorphological mapping: A review of approaches and frameworks for best practice.* Earth Science Reviews 185, 806-846. https://doi.org/10.1016/j.earscirev.2018.07.015

Çiner, A. and Sarıkaya, M.A. (2017). Cosmogenic 36Cl Geochronology of late Quaternary glaciers on the Bolkar Mountains, south central Turkey. IN: P., Hughes & J., Woodward (Eds.). Quaternary

Glaciation in the Mediterranean Mountains. London: Geological Society of London Special Publications 433, pp. 271-287. https://doi.org/10.1144/SP433.3

Clark ,P.U., Dyke, A.S., Shakun, J.D., Carlson, A.E., Clark, J., Wohlfarth, B., Mitrovica, J.X., Hostetler, S.W., McCabe. A.M. (2009). The Last Glacial Maximum. *Science 325*, 710-714. https://doi.org/10.1126/science.1172873Clark

D'Arcy, M., Schildgen, T.F., Strecker, M.R., Wittmann, H., Duesing, W., Mey, J., Tofelde, S., Weissmann, P., Alonso, R.N. (2019). Timing of past glaciation at the Sierra de Aconquija, northwestern Argentina, and throughout the Central Andes. *Quaternary Science Reviews 204*, 37-57. https://doi.org/10.1016/j.quascirev.2018.11.022

Darvill, C.M. (2013). Cosmogenic nuclide analysis. IN: *Geomorphological Techniques* (pp. 1-25). London: British Society for Geomorphology. http://geomorphology.org.uk/sites/default/files/geom_tech_chapters/4.2.10_CosmogenicNuclideAnalysis.pdf

De Martini, P.M., Pantosti, D., Palyvos, N., Lemeille, F., McNeill, L.C., Collier, R.E.L. (2004). Slip rates of the Aigion and Eliki Faults from uplifted marine terraces, Corinth Gulf, Greece. *Comptes Rendus Geoscience 336*, 325–334. http://doi.org/10.1016/j.crte.2003.12.006

Desilets, D., Zreda, M., Almasi, P.F., Elmore, D., (2006). Determination of cosmogenic $^{36}$Cl in rocks by isotope dilution: innovations, validation and error propagation. *Chemical Geology 233*, 185-195. https://doi.org/10.1016/j.chemgeo.2006.03.001

Dilek, Y., Kempton, P.D., Thy, P., Hurst, S.D., Whitney, D., and Kelley, D.S. (1997). Structure and petrology of hydrothermal veins in gabbroic rocks from Sites 921 to 924, MARK area (Leg 153): alteration history of slow-spread lower oceanic crust. IN: Karson, J.A., Cannat, M., Miller, D.J., and Elthon, D. (Eds.), *Proc. ODP, Sci. Results,153: College Station, TX (Ocean Drilling Program)*. doi:10.2973/odp.proc.ir.153.1995

Dupuy, C., Dostal, J., Capedri, S., Venturelli, G. (1984). Geochemistry and petrogenesis of ophiolites from Northern Pindos (Greece). *Bulletin of Volcanology 47*, 39-46. https://doi.org/10.1007/BF01960539

Finkel, R. C., Owen, L. A., Barnard, P. L., Caffee, M. W. (2003). Beryllium-10 dating of Mount Everest moraines indicates a strong monsoonal influence and glacial synchroneity throughout the Himalaya. *Geology 31*, 561–564. https://doi.org/10.1130/0091-7613(2003)031<0561:BDOMEM>2.0.CO;2

Frogley, M.R. (1998). *The Biostratigraphy, Palaeoecology and Geochemistry of a Long Lacustrine Sequence from NWGreece* (Thesis). Cambridge: University of Cambridge. https://doi.org/10.17863/CAM.16400

Fotiadi, A.K., Metaxas, D.A. and Bartzokas, A. (1999). A statistical study of precipitation in northwest Greece. *International Journal of Climatology 19*, 1221-1232. https://doi.org/10.1002/(SICI)1097-0088(199909)19:11<1221::AID-JOC436>3.0.CO;2-HFurlan, D. (1977). The Climate of Southeast Europe. IN: Wallen, C.C. (ed.) *Climates of Central and Southern Europe*. Elsevier: Amsterdam. p. 185-223.

Galanidou, N., Tzedakis, P.C., Lawson, I.T., Frogley, M.R. (2000). A revised chronological and paleoenvironmental framework for the Kastritsa rockshelter, northwest Greece. Antiquity 74, 349-355. https://doi.org/10.1017/S0003598X00059421

Garcia-Ruiz, J.M., Moreno, A., Gonzalez-Samperiz, P., Valero-Garces, B.L., Marti-Bono, C. (2010). La cronologia del ultimo ciclo glaciar en las montanas del Sur de Europa. Una revision. *Revista Cuaternario y Geomorfología 24*, 35–46.

Giraudi, C. (2012). The Campo Felice Late Pleistocene glaciation (Apennines, central Italy). *Journal of Quaternary Science 27*, 432-440. https://doi.org/10.1002/jqs.1569.

878 Giraudi, C. and Giaccio, B. (2015). Middle Pleistocene glaciations in the Apennines, Italy: new
879 chronological data and preservation of the glacial record. IN: Hughes, P.D. and Woodward, J.C.
880 (eds), *Quaternary Glaciation in the Mediterranean Mountains*. London: Geological Society of
881 London Special Publications 433, pp. 161-178. https://doi.org/10.1144/SP433.1
882 Gómez-Ortiz, A., Palacios, D., Palade, B., Vazquez-Selem, L., Salvador-Franch, F. (2012). The
883 deglaciation of the Sierra Nevada (Southern Spain). *Geomorphology 159-160*, 93-105.
884 https://doi.org/10.1016/j.geomorph.2012.03.008
885 Gosse, J.C. and Phillips, F.M. (2001) Terrestrial in situ cosmogenic nuclides: theory and application.
886 *Quaternary Science Reviews 20*, 1475-1560. https://doi.org/10.1016/S0277-3791(00)00171-2
887 Gosse, J.C., Klein, J., Evenson, E.B., Lawn, B., Middleton, R. (1995). Beryllium-10 dating of the
888 duration and retreat of the last Pinedale glacial sequence. *Science 268*, 1329-1333
889 https://doi.org/10.1126/science.268.5215.1329
890 Gouvas, M. and Sakellariou, N. (2011). Climate and forest vegetation of Greece. National
891 Observatory of Athens, Institute of Environmental Research and Sustainable Development,
892 Technical Library Report Nr: 01/2011 (in Greek).
893 Hamlin, R.H.B., Woodward, J.C., Black, S., Macklin, M.G. (2000). Sediment fingerprinting as a tool
894 for interpreting long-term river activity: the Voidomatis basin, Northwest Greece In: Foster, I.D.L.
895 (Eds.), *Tracers in Geomorphology*. Chichester, UK: Wiley, pp. 473–501.
896 Hedding, D. W., and Sumner, P. D. (2013). Diagnostic Criteria for pronival ramparts: Site,
897 Morphological and sedimentological characteristics. *Geografiska Annaler. Series A, Physical*
898 *Geography*, *95*, 315–322. http://www.jstor.org/stable/43870695
899 Heyman, J., Stroeven A.P., Harbor, J.M., Caffee, M.W. (2011). Too young or too old: Evaluating
900 cosmogenic exposure dating based on an analysis of compiled boulder exposure ages. *Earth and*
901 *Planetary Science Letters 302*, 71-80. https://doi.org/10.1016/j.epsl.2010.11.040
902 Hughes P.D. (2004). Quaternary glaciation in the Pindus Mountains, northwest Greece. PhD thesis,
903 University of Cambridge.
904 Hughes, P.D. (2007). Recent behaviour of the Debeli Namet glacier, Durmitor, Montenegro. *Earth*
905 *Surface Processes and Landforms 10*, 1593-1602. https://doi.org/10.1002/esp.1537
906 Hughes, P.D. (2010a). Little Ice Age glaciers in Balkans: low altitude glaciation enabled by cooler
907 temperatures and local topoclimatic controls. *Earth Surface Processes and Landforms 35*, 229–
908 241. https://doi.org/10.1002/esp.1916
909 Hughes, P.D. (2010b). Geomorphology and Quaternary stratigraphy: The roles of morpho-, litho-, and
910 allostratigraphy. *Geomorphology 123*, 189-199. https://doi.org/10.1016/j.geomorph.2010.07.025
911 Hughes, P.D. and Gibbard, P.L. (2015). A stratigraphical basis for the Last Glacial Maximum (LGM).
912 *Quaternary International 383*, 174-185.
913 Hughes, P.D., Woodward, J.C., Gibbard, P.L., Macklin, M.G., Gilmour, M.A., Smith G.R. (2006a).
914 The glacial history of the Pindus Mountains, Greece. *Journal of Geology 114*, 413-434.
915 Hughes, P.D., Woodward, J.C., Gibbard, P.L. (2006b). Middle Pleistocene glacier behaviour in the
916 Mediterranean: sedimentological evidence from the Pindus Mountains, Greece. *Journal of the*
917 *Geological Society, London 163*, 857-867.
918 Hughes, P.D., Woodward J.C., Gibbard, P.L. (2006c). Late Pleistocene glaciers and climate in the
919 Mediterranean, *Global and Planetary Change 50*, 83-98.
920 https://doi.org/10.1016/j.gloplacha.2005.07.005
921 Hughes P.D., Woodward, J.C., Gibbard, P.L. (2006d). The last glaciers of Greece. *Zeitscrift fuer*
922 *Geomorphologie 50*, 37-46.
923 Hughes, P.D., Woodward, J.C., van Calsteren, P.C., Thomas, L.E., Adamson, K.R. (2010).
924 Pleistocene ice caps on the coastal mountains of the Adriatic Sea: palaeoclimatic and wider

palaeoenvironmental implications. *Quaternary Science Reviews 29*, 3690–3708. https://doi.org/10.1016/j.quascirev.2010.06.032

Hughes, P.D., Woodward, J.C., van Calsteren, P.C., Thomas, L.E. (2011). The glacial history of the Dinaric Alps, Montenegro. *Quaternary Science Reviews 30*, 3393–3412. https://doi.org/10.1016/j.quascirev.2011.08.016

IGME (Institute of Geology and Mineral Exploration) (1959) 1:50,000 Geological map of Greece. Metsovon Sheet. Institute of Geological and Mineral Exploration, Athens.

Ivy-Ochs, S. and Kober, F. (2008). Surface exposure dating with cosmogenic nuclides. E&G Quaternary Science Journal 57, 179–209. https://doi.org/10.3285/eg.57.1-2.7

Ivy-Ochs, S. and Briner, J. (2014). Dating disappearing ice with cosmogenic nuclides. *Elements 10*, 351–356. https://doi.org/10.2113/gselements.10.5.351

Ivy-Ochs, S., Kerschner, H., Kubik, P.W., Schlüchter, C. (2006a). Glacier response in the European Alps to Heinrich Event 1 cooling: the Gschnitz stadial. *Journal of Quaternary Science 21*, 115–130. https://doi.org/10.1002/jqs.955

Ivy-Ochs, S., Kerschner, H., Reuther, A., Maisch, M., Sailer, R., Schaefer, J., Kubik, P.W., Synal, H.-A., Schlüchter, C. (2006b). The timing of glacier advances in the northern European Alps based on surface exposure dating with cosmogenic $^{10}$Be, $^{26}$Al, $^{36}$Cl, and $^{21}$Ne. IN: Alonso-Zarza, A.M., Tanner, L.H. (Eds.). *In Situ-Produced Cosmogenic Nuclides and Quantification of Geological Processes.* Geological Society of America, Special Paper 415. https://doi.org/10.1130/2006.2415(04)

Ivy-Ochs, S., Kerschner, H., Schlüchter, C. (2007). Cosmogenic nuclides and the dating of Lateglacial and Early Holocene glacier variations: The Alpine perspective. *Quaternary International 164-165*, 53-63. https://doi.org/10.1016/j.quaint.2006.12.008

Jones, G. and Robertson, A.H.F. (1991). Tectono-stratigraphy and evolution of the Mezozoic Pindus ophiolite and related units, northwestern Greece. *Journal of the Geological Society, London 148*, 267–288. https://doi.org/10.1144/gsjgs.148.2.0267

Katsoulakos, N.M. and Kaliampakos, D.C. (2014). What is the impact of altitude on energy demand? A step towards developing specialized energy policy for mountainous areas. *Energy Policy 71*, 130-138. https://doi.org/10.1016/j.enpol.2014.04.003

Kelemen, P., Kikawa, E., Miller, J., Abe, N., Bach, W., Carlson, R.L., Casey, J.F., Chambers, L.M., Cheadle, M., Cipriani, A., Dick, H.J.B., Faul, U., Garces, M., Garrido, C., Gee, J.S.,Godard, M., Griffin, D.W., Harvey, J., Ildefonse, B., Iturrino, G.J., Josef, J., Meurer, W.P.,Paulick, H., Rosner, M., Schroeder, T., Seyler, M., Takazawa, E. (2004). Site 1268. In Kelemen, P.B., Kikawa, E., Miller, D.J., et al., *Proc. ODP, Init. Repts., 209: College Station, TX (Ocean Drilling Program)*, 1–171. doi:10.2973/odp.proc.ir.209.103.2004

Kelemen, P., Matter, J., Streit, E., Rudge, J., Curry, W.B., Blusztajn, J. (2011). Rates and Mechanisms of Mineral Carbonation in Peridotite: Natural Processes and Recipes for Enhanced, in situ $CO_2$ Capture and Storage. *Annual Review of Earth and Planetary Sciences 39*, 545-576. https://doi.org/10.1146/annurev-earth-092010-152509

King, G. and Bailey, G. (1985). The palaeoenvironment of some archaeological sites in Greece: the influence of accumulated uplift in a seismically active region. *Proceedings of the Prehistoric Society 51*, 273–282. https://doi.org/10.1017/S0079497X0000712X

Köse, O., Sarıkaya, M.A., Çiner, A., Candaş, A. (2019). Late Quaternary glaciations and cosmogenic 36Cl geochronology of Mount Dedegöl, south-west Turkey. *Journal of Quaternary Science 34*, 51-63. https://doi.org/10.1002/jqs.3080

Leontaritis, A.D. (2021). The Late Quaternary Glacial History of Greece. PhD thesis, Harokopio University of Athens, Greece. https://doi.org/10.13140/RG.2.2.15282.02240

Leontaritis, A.D., Kouli, K. & Pavlopoulos, K. (2020). The glacial history of Greece: a comprehensive review. *Mediterranean Geoscience Reviews 2*, 65–90. https://doi.org/10.1007/s42990-020-00021-w

Lewin, J., Macklin, M. G., Woodward, J.C. (1991). Late Quaternary fluvial sedimentation in the Voidomatis Basin, Epirus, northwest Greece. *Quaternary Research 35*, 103–115. https://doi.org/10.1016/0033-5894(91)90098-P

Li, Y. (2018). Determining topographic shielding from digital elevation models for cosmogenic nuclide analysis: a GIS model for discrete sample sites. *Journal of Mountain Science 15*, 939–947. https://doi.org/10.1007/s11629-018-4895-4

Lifton, N., Sato, T., Dunai, T.J. (2014). Scaling in situ cosmogenic nuclide production rates using analytical approximations to atmospheric cosmic-ray fluxes. *Earth and Planetary Science Letters 386*, 149-160. https://doi.org/10.1016/j.epsl.2013.10.052

Louis, H. (1926). Glazialmorphologishche Beobachtungen im albanischen Epirus. *Zeitschrift der Gesellschaft für Erdkunde 1926*, 398–409.

Lowe, J.J. and Walker, M.J.C. (1997). *Reconstructing Quaternary environments.* London: Longman, pp. 446.

Lukas, S. (2006). Morphostratigraphic principles in glacier reconstruction – a perspective from the British Younger Dryas. *Progress in Physical Geography 30*, 719–736. https://doi.org/10.1177/0309133306071955

Macklin, M.G. and Woodward, J.C. (2009). Rivers and environmental change. In: Woodward, J.C. (Ed.). *The Physical Geography of the Mediterranean.* Oxford: Oxford University Press, pp. 319-252.

Macklin, M.G., Lewin, J., Woodward, J.C. (1997). Quaternary river sedimentary sequences of the Voidomatis basin. IN: Bailey, G.N. (Ed.), *Klithi: Palaeolithic Settlement and Quaternary Landscapes in Northwest Greece (*pp. 347-359). Cambridge: McDonald Institute.

Marrero, S.M., Phillips, F.M., Caffee, M.W., Gosse, J.C. (2016a). CRONUS-Earth cosmogenic $^{36}$Cl calibration. *Quaternary Geochronology 31*, 199-219. https://doi.org/10.1016/j.quageo.2015.10.002

Marrero, S.M., Phillips, F.M., Borchers, B., Lifton, N., Aumer, R., Balco, G. (2016b). Cosmogenic nuclide systematics and the CRONUScalc program. *Quaternary Geochronology 31*, 160-187. https://doi.org/10.1016/j.quageo.2015.09.005.

Marrero, S.M., Phillips, F.M., Caffee, M.W., Gosse, J.C. (2021). Corrigendum to 'CRONUS-Earth cosmogenic $^{36}$Cl calibration [Quaternary Geochronology 31 (2016) 199–219]'. *Quaternary Geochronology 61*, 101130. https://doi.org/10.1016/j.quageo.2020.101130

Masarik, J. and Wieler, R., 2003. Production rates of cosmogenic nuclides in boulders. *Earth and Planetary Science Letters*, *216*, 201-208. https://doi.org/10.1016/S0012-821X(03)00476-X

Matthews, J., Wilson, P., Mourne, R. (2017) Landform transitions from pronival ramparts to moraines and rock glaciers: a case study from the Smørbotn cirque, Romsdalsalpane, southern Norway, *Geografiska Annaler: Series A, Physical Geography 99*, 15-37. https://doi.org/10.1080/04353676.2016.1256582

McNeill, L.C. and Collier, R.E.L. (2004). Uplift and slip rates of the eastern Eliki fault segment, Gulf of Corinth, Greece, inferred from Holocene and Pleistocene terraces 1. *Journal of the Geological Society London 161*, 81–92. http://doi.org/10.1144/0016-764903-029

Mistardis, G. (1935). *Geomorphological research in northeastern Epirus* (In Greek). Athens, Greece: Hellenic Geographical Society

Moore, A.K. and Granger, D.E. (2019). Calibration of the production rate of cosmogenic $^{36}$Cl from Fe. *Quaternary Geochronology 51*, 87-98. https://doi.org/10.1016/j.quageo.2019.02.002

Niculescu, C. (1915). Sur les traces de glaciation dans le massif Smolica chaıne du Pinde meridional. *Bulletin de la Section Scientifique de l'Academie Roumaine 3*, 146–151.

Oerlemans, J. (2005). Extracting a climate signal from 169 glacier records. *Science 308*, 675–677. https://doi.org/10.1126/science.1107046

Ohmura A. and Boetcher, M. (2018). Climate on the equilibrium line altitudes of glaciers: Theoretical background behind Ahlmann's P/T diagram. *Journal of Glaciology 64*, 489-505.

Oliva, M., Palacios, D., Fernández-Fernández, J. M., Rodríguez-Rodríguez, L., Garcia Ruiz, J-M., Andrés, N., Carrasco, R. M., Pedrazza, J., Perez Alberti, A., Valcarel, M., Hughes, P.D. (2019). Late Quaternary glacial phases in the Iberian Peninsula. *Earth Science Reviews 192*, 564-600. https://doi.org/10.1016/j.earscirev.2019.03.015

Osmaston, H.A. (2005). Estimates of glacier equilibrium line altitudes by the Area×Altitude, theArea×Altitude Balance Ratio and the Area×Altitude Balance Index methods and their validation. *Quaternary International 138–139*, 22–31. https://doi.org/10.1016/j.quaint.2005.02.004

Owen, L. A., Finkel, R. C., Caffee, M. W. (2002). A note on the extent of glaciation throughout the Himalaya during the global Last Glacial Maximum. *Quaternary Science Reviews 21*, 147–157. https://doi.org/10.1016/S0277-3791(01)00104-4

Palacios, D., Gomez-Ortiz, A., Andres, N., Salvador, F., Oliva, M., (2016). Timing and ne geomorphologic evidence of the Last Deglaciation stages in Sierra Nevada (southern Spain). Quaternary Science Reviews 150, 110–129. https://doi.org/10.1016/j.quascirev.2016.08.012

Palmentola, G., Boenzi, F., Mastronuzzi, G., Tromba, F. (1990). Osservazioni sulle trace glaciali del M. Timfi, Catena del Pindo (Grecia). Geografia Fisica e Dinamica Quaternaria 13, 165–170.

Papada, L. and Kaliampakos, D. (2016). Developing the energy profile of mountainous areas. *Energy 107*, 205-214. https://doi.org/10.1016/j.energy.2016.04.011

Pellitero, R., Rea, B.,R., Spagnolo, M., Bakke, J., Hughes, P., Ivy-Ochs, S., Lukas, S., Ribolini, A. (2015). A GIS tool for automatic calculation of glacier equilibrium-line altitudes. *Computer & Geosciences 82*, 55–62. https://doi.org/10.1016/j.cageo.2015.05.005

Pellitero, R., Rea, B.,R., Spagnolo, M., Bakke, J., Ivy-Ochs, S., Frew, C. R., Hughes, P., Ribolini, A., Lukas, S., Renssen, H., 2016. GlaRe a GIS tool to reconstruct the 3D surface of palaeoglaciers. *Computer & Geosciences 94*, 77-85. https://doi.org/10.1016/j.cageo.2016.06.008

Pelletier, L., Vils, F., Kalt, A., Gméling, K. (2008). Li, B and Be Contents of Harzburgites from the Dramala Complex (Pindos Ophiolite, Greece): Evidence for a MOR-type Mantle in a Supra-subduction Zone Environment. *Journal of Petrology* 49, *2043*–2080. https://doi.org/10.1093/petrology/egn057

Phillips, F., Argento, D., Balco, G., Caffee, M., Clem, J., Dunai, T., Finkel, R., Goehring, B., Gosse, J., Hudson, A., Jull, A., Kelly, M., Kurz, M., Lal, D., Lifton, N., Marrero, S.M., Nishiizumi, K., Reedy, R.C., Schaefer, J.M., Stone, J., Swanson, T., Zreda, M. (2016). The CRONUS-Earth Project: A synthesis. *Quaternary Geochronology*, *31*, 119-154. https://doi.org/10.1016/j.quageo.2015.09.006

Phillips, F.M., Stone, W.D., Fabryka-Martin, J. (2001). An improved approach to calculating low-energy cosmic-ray neutron fluxes near the land/atmosphere interface, *Chemical Geology 175*, 689–701. https://doi.org/10.1006/qres.2001.2278Pope, R.J., Hughes, P.D., Skourtsos, E. (2017). Glacial history of Mount Chelmos, Peloponnesus, Greece. IN: Hughes, P.D. and Woodward, J.C. (Eds.), *Quaternary Glaciation in the Mediterranean Mountains.* London: Geological Society of London Special Publications 433, pp. 211-236. https://doi.org/10.1144/SP433.11

Rasmussen, S.O., Andersen, K.K., Svensson, A.M., Steffensen, J.P., Vinther, B.M., Clausen, H.B., Siggaard-Andersen, M.-L., Johnsen, S.J., Larsen, L.B., Dahl- Jensen, D., Bigler, M., Roethlisberger, R., Fischer, H., Goto-Azuma, K., Hansson, K.J., M.E., Ruth, U. (2006). A new Greenland ice core chronology for the last glacial termination. *Journal of Geophysical Research 111 (D06102)*, 1-16. https://doi.org/10.1029/2005JD006079

Rasmussen, S.O., Bigler, M., Blockley, S. P., Blunier, T., Buchardt, S.L., Clausen, H. B., Cvijanovic, I., Dahl-Jensen, D., Johnsen, S.J., Fischer, H., Gkinis, V., Guillevic, M., Hoek, W.Z., Lowe, J.J., Pedro, J.B., Popp, T., Seierstad, I.K., Steffensen, J.P., Svensson, A.M., Vallelonga, P., Vinther, B.M.,Walker, M.J.C., Wheatley, J.J., Winstrup, M. (2014). A stratigraphic framework for abrupt climatic changes during the Last Glacial period based on three synchronized Greenland ice-core records: refining and extending the INTIMATE event stratigraphy. *Quaternary Science Reviews 106*, 14-28. https://doi.org/10.1016/j.quascirev.2014.09.007

Rea, B.R. (2009). Defining modern day Area–Altitude Balance Ratios (AABRs) and their use in glacier–climate reconstructions. *Quaternary Science Reviews 28*, 237–248. https://doi.org/10.1016/j.quascirev.2008.10.011

Richards, B.W.M., Benn, D.I., Owen, L.A., Rhodes, E.J. and Spencer, J.Q.G. (2000). Timing of late Quaternary glaciations south of Mount Everest in the Khmubu Himal, Nepal. *Geological Society of America Bulletin 112*, 1621–32. https://doi.org/10.1130/0016-7606(2000)112<1621:TOLQGS>2.0.CO;2

Robertson, A. H. F. (2002). Overview of the genesis and emplacement of Mesozoic ophiolites in the Eastern Mediterranean Tethyan region. *Lithos 65*, 1–67. https://doi.org/10.1016/S0024-4937(02)00160-3

Rodriguez-Rodriguez, L., Jimenez-Sanchez, M., Dominguez-Cuesta, M.J., Rico, M.T., Valero-Garces, B.L. (2011). Last deglaciation in northwestern Spain: New chronological and geomorphologic evidence from the Sanabria region. *Geomorphology 135*, 48–65. https://doi.org/10.1016/j.geomorph.2011.07.025

Sanchez Goñi, M.F., Harrison, S.P. (2010). Millennial-scale climate variability and vegetation changes during the Last Glacial: concepts and terminology. *Quaternay Science Reviews 29*, 2823-2827. https://doi.org/10.1016/j.quascirev.2009.11.014

Sarıkaya, M. A., Zreda, M., Çiner, A., Zweck, C. (2008). Cold and wet Last Glacial Maximum on Mount Sandıras, SW Turkey, inferred from cosmogenic dating and glacier modeling. *Quaternary Science Reviews 27*, 769-780. https://doi.org/10.1016/j.quascirev.2008.01.002

Sarıkaya, M.A., Ciner, A., Haybat, H., Zreda, M. (2014). An early advance of glaciers on Mount Akdag˘, SW Turkey, before the global Last Glacial Maximum; insights from cosmogenic nuclides and glacier modelling. *Quaternary Science Reviews 88*, 96-109. https://doi.org/10.1016/j.quascirev.2014.01.016

Sarıkaya, M.A., Stepišnik, U., Žebre, M., Çiner, A., Yıldırım, C., Vlahović, I., Tomljenović, B., Matoš, B., Wilcken , K.M. (2020). Last glacial maximum deglaciation of the Southern Velebit Mt. (Croatia): insights from cosmogenic $^{36}$Cl dating of Rujanska Kosa. *Mediterranean Geoscience Reviews 2*, 53–64. https://doi.org/10.1007/s42990-020-00030-9

Schimmelpfennig, I., Benedetti, L., Finkel, R., Pik, R., Blard, P. H., Bourles, D., Burnard, P., Williams, A. (2009). Sources of in-situ 36Cl in basaltic rocks. Implications for calibration of production rates. Quaternary Geochronology 4, 441–461. https://doi.org/10.1016/j.quageo.2009.06.003

Schimmelpfennig, I., Benedetti, L., Garreta, V., Pik, R., Blard, P-H., Burnard, P., Bourles, D., Finkel, R., Ammon, K., Dunai, T. (2011). Calibration of cosmogenic 36Cl production rates from Ca and K spallation in lava flows from Mt. Etna (38o, Italy) and Payun Matru (36 o S, Argentina). Geochimica et Cosmochimica Acta 75, 2611-2632. https://doi.org/10.1016/j.gca.2011.02.013

Sestini, A. (1933). Tracce glaciali sul Pindo epirota. *Bollettino della Reale Societa` Geografica Italiano 10*, 136–156.

Shakun, J.D., Clark, P.U., He, F., Lifton, N.A., Liu, Z., Otto-Bliesner, B.L. (2015). Regional and global forcing of glacier retreat during the last deglaciation. *Nature Communications 6*, 8059. https://doi.org/10.1038/ncomms9059

Sharma, P., Kubik, P.W., Fehn, U., Gove, H.E., Nishiizumi, K., Elmore, D., (1990). Development of $^{36}$Cl standards for AMS. *Nuclear Instruments and Methods in Physics Research Section B: Beam Interactions with Materials and Atoms 52*, 410-415. https://doi.org/10.1016/0168-583X(90)90447-3

Styllas M.N., Schimmelpfennig, I., Benedetti, L., Ghilardi, M., Aumaître, G., Bourlès, D., Keddadouche, K. (2018). Late-glacial and Holocene history of the northeast Mediterranean mountain glaciers - New insights from in situ-produced $^{36}$Cl-based cosmic ray exposure dating of paleo-glacier deposits on Mount Olympus, Greece. *Quaternary Science Reviews 193,* 244-265. https://doi.org/10.1016/j.quascirev.2018.06.020

Svendsen, J. I., Alexanderson, H., Astakhov, V. I., Demidov, I., Dowdeswell, J. A., Funder, S., Gataullin, V., Henriksen, M., Hjort, Ch., Houmark-Nielsen, M., Hubberten, H. W., Ingo´ lfsson, O., Jakobsson, M., Kjær, K. H., Larsen, E., Lokrantz, H., Lunkka, J. P., Lysa˚ , A., Mangerud, J., Matiouchkov, A., Murray, A. S., Moeller, P., Niessen, F., Nikolskaya, O., Polyak, L., Saarnisto, M., Siegert, Ch., Siegert, M. J., Spielhagen, R. F., Stein, R. (2004). Late Quaternary ice sheet history of northern Eurasia. *Quaternary Science Reviews 23,* 1229–1271. https://doi.org/10.1016/j.quascirev.2003.12.008

Swanson, T.W. and Caffee, M.L. (2001). Determination of $^{36}$Cl Production Rates Derived from the Well-Dated Deglaciation Surfaces of Whidbey and Fidalgo Islands, Washington. *Quaternary Research 56*, 366–382. https://doi.org/10.1006/qres.2001.2278

Tzedakis, P.C., Lawson, I.T., Frogley, M.R., Hewitt, G.M., Preece, R.C. (2002). Buffered tree population changes in a Quaternary refugium: evolutionary implications. *Science 297*, 2044-47. https://doi.org/10.1126/science.1080630

Tzedakis, P.C., McManus, J.F., Hooghiemstra, H., Oppo, D.W., Wijmstra, T.A. (2003). Comparison of changes in vegetation in northeast Greece with records of climate variability on orbital and suborbital frequencies over the last 450 000 years. *Earth and Planetary Sciece Letters 212*, 197-212. https://doi.org/10.1016/S0012-821X(03)00233-4

Vogiatzakis, I.N. (2012). *Mediterranean Mountain Environments.* Oxford: Wiley-Blackwell.

Woodward, J.C. (2009). *The Physical Geography of the Mediterranean.* Oxford: Oxford University Press.

Woodward, J.C. and Hughes, P.D. (2011). Glaciation in Greece: A New Record of Cold Stage Environments in the Mediterranean. IN: Ehlers J., Gibbard, P.L., Hughes, P.D. (Eds.), *Quaternary glaciations - Extent and chronology. A closer look.* (pp. 175-198). Amsterdam: Elsevier. https://doi.org/10.1016/B978-0-444-53447-7.00015-5

Woodward, J.C., Macklin, M.G., Smith, G.R. (2004). Pleistocene glaciation in the mountains of Greece. IN: Ehlers J., Gibbard, P.L. (Eds.), *Quaternary glaciations - extent and chronology. Part I: Europe.* Amsterdam: Elsevier, pp. 155-173. https://doi.org/10.1016/S1571-0866(04)80066-6